Argonne
NATIONAL LABORATORY

ANL-07/16

Dynamic Modeling Efforts for System Interface Studies for Nuclear Hydrogen Production

Nuclear Engineering Division

About Argonne National Laboratory

Argonne is a U.S. Department of Energy laboratory managed by UChicago Argonne, LLC under contract DE-AC02-06CH11357. The Laboratory's main facility is outside Chicago, at 9700 South Cass Avenue, Argonne, Illinois 60439. For information about Argonne, see www.anl.gov.

Availability of This Report

This report is available, at no cost, at http://www.osti.gov/bridge. It is also available on paper to the U.S. Department of Energy and its contractors, for a processing fee, from:

U.S. Department of Energy
Office of Scientific and Technical Information
P.O. Box 62
Oak Ridge, TN 37831-0062
phone (865) 576-8401
fax (865) 576-5728
reports@adonis.osti.gov

ANL-07/16

Dynamic Modeling Efforts for System Interface Studies for Nuclear Hydrogen Production

by
R.B. Vilim
Nuclear Engineering Division, Argonne National Laboratory

December 2006

TABLE OF CONTENTS

LIST OF FIGURES

LIST OF TABLES

ABSTRACT

DYNAMIC MODELING EFFORTS FOR SYSTEM INTERFACE STUDIES

by

R. B. VILIM

System interface studies require not only identifying economically optimal equipment configurations, which involves studying mainly full power steady-state operation, but also assessing the operability of a design during load change and startup and assessing safety-related behavior during upset conditions. This latter task is performed with a dynamic simulation code. This report reviews the requirements of such a code. It considers the types of transients that will need to be simulated, the phenomena that will be present, the models best suited for representing the phenomena, and the type of numerical solution scheme for solving the models to obtain the dynamic response of the combined nuclear-hydrogen plant.

Useful insight into plant transient behavior prior to running a dynamics code is obtained by some simple methods that take into account component time constants and energy capacitances. Methods for determining reactor stability, plant startup time, and temperature response during load change, and tripping of the reactor are described. Some preliminary results are presented.

I. INTRODUCTION

Two important issues arise in the design of the interface between the reactor and chemical plant for the production of hydrogen using nuclear power. The first is an economic issue and involves identifying plant configurations with high efficiency while striking a balance with any accompanying increase in plant cost. This issue is addressed with the aid of a steady-state code such as HyPEP [1]. In addition to identifying economically optimal equipment configurations, which involves studying full-power steady-state operation, there is also a need to assess the operability of a design during load change and startup and to assess safety-related behavior during upset conditions. This second issue is examined with a dynamic simulation code and involves investigating whether process variables remain within limits during these transients.

Work has begun on developing a dynamic simulation capability for the Very High Temperature Reactor (VHTR) coupled to the High Temperature Electrolysis (HTE) process. This report reviews as part of that task candidate modeling approaches and numerical methods for obtaining a solution for the integrated plant behavior

Prior to running such a computer code some useful insight into dynamic behavior is obtained by simple methods that take into account component time constants and energy capacitances. This report describes analytic methods that have been used to assess important time-related behavior including plant stability and temperature rates of change. These studies were performed in advance of dynamic simulations and serve as an aid to determining the types of transient to be run. Preliminary results are given for operational and upset events.

II. COMPONENTS AND PHENOMENA

A key step in developing a dynamic simulation capability is to identify the types of equipment components that appear and the important phenomena in each. This requires first identifying the spectrum of plants and transients that are to be simulated. In this project the plant is the Very High Temperature Reactor (VHTR) coupled to the High Temperature Electrolysis (HTE) process and to the sulfur iodine (SI) process. Both plant combinations are leading candidates for DOE demonstration of nuclear hydrogen production. Presently, the HTE process is better characterized and so this report focuses mainly on it. The SI process and the types of models needed will be examined at a later time. The transients to be simulated follow from the project goal which is to develop a code that can be used to study equipment configurations for producing nuclear hydrogen in a cost effective and practical manner. This necessarily requires being able to simulate load change, startup/shutdown, and anticipated upset transients. Simulation of severe accidents (i.e. transients where process variables range outside of safety limits and consequently equipment is damaged) is not included. Such accidents will need to be analyzed at some point, but they should not drive the plant design at this time.

In part what must be done parallels the preparation of Phenomena Identification and Ranking Tables (PIRTs) for code development for safety analyses of reactors.[2] PIRTs identify the most important phenomena and are an aid to efficient allocation of modeling effort. In a nutshell, for each transient, one identifies the components that participate and the phenomena. The

phenomena are ranked in order of importance for each transient. In this report an abbreviated version of a PIRT is generated. Phenomena are listed by component and ordered into two classes. In the first class are those phenomena that could be considered basic and required for accurate prediction of startup, load change, and anticipated upset transient. In the second class are those phenomena whose representation is not crucial for accurate transient simulation. This binary ranking of phenomena by component is given in Table I. It provides a basis in Section IV for making some preliminary assessments of what to include in a dynamic simulation code. One notes that the terms *phenomena* and *models* are somewhat interchangeable. To identify and describe a phenomenon in a meaningful engineering sense one must first be able to identify a "cause and effect". Whether the description is empirical involving measured correlations among variables or is based on fundamental heat, mass, and momentum transport processes, both amount to having created a model or representation.

III. MODEL FORMS AND SOLUTION

Whether phenomena are represented as empirical correlations or by fundamental transport processes has implications for model forms and how they are solved. The basic framework remains the conservation of mass, energy, and momentum. However, an empirical representation implies lumping of space which leads to ordinary differential equations (ODE) while representation by fundamental transport processes implies partial differential equations (PDE). This section describes these two cases with the goal of identifying in Section IV an appropriate treatment for system interface studies.

A. Partial Differential Equations

In the PDE approach conservation balances for mass, energy, and momentum are written for an infinitesimal control volume. The result is a partial differential equation of the general form [3]

$$\frac{\partial}{\partial t}(\rho\phi) + \nabla\cdot(\rho\boldsymbol{u}\phi) = \nabla\cdot(\Gamma_\phi\nabla\phi) + S_\phi \qquad (1)$$

where time and space are independent variables and where ρ is density, ϕ is the dependent variable, $\boldsymbol{u}$ is velocity, Γ is a diffusion coefficient, and S is a source term. For the mass balance the dependent variable is unity, for the energy balance it is internal energy, and for the momentum balance it is velocity. The four terms in the above equation represent, respectively, the rate of change of the conserved quantity within the control volume, the rate of convection out, the rate of diffusion in, and the internal production rate. The Γ term represents diffusion-based transport processes while the S terms is intended to take in those other transport processes, such as turbulent shear, that do not fit the form of the Γ term.

A.1 Discretization

To obtain the dependent variable ϕ as a function of time and space the above equation must be integrated. A grid is laid out over the region of space of interest. The grid lines (2-D) or planes (3-D) define a set of non-overlappping control volumes with a grid point at the center of each

Table I Listing of Phenomena by Component

Process Elements	Component	Phenomena as Characterized by Level of Representation	
		Empirical	Fundamental Transport
Analytical Mechanics	Rotating Shaft	-	Solid body rotation.
Heat Transfer/Fluid Flow	Pipe/Plenum	Friction factor, 1-D	Boundary layer, Turbulence, Heat diffusion, 3-D
	Turbine/Compressor	Loss correlations, 1-D	Boundary layer, 3-D
	Heat Exchanger	Friction factor, Heat transfer coefficient, Radiation view factors,1-D	Boundary layer, Turbulence, Differential radiation view factors, 3-D
	Boiler/Condenser	Friction factor, Heat transfer coefficient, Phase equilibrium,1-D	Boundary layer, Turbulence, Phase non-equilibrium, 3-D
Heat Transfer/Fluid Flow/Neutronics	Reactor Core	Friction factor, Heat transfer coefficient, Radiation view factors, Point Kinetics, 1-D	Boundary layer, Turbulence, Differential radiation view factors, Space-time kinetics, 3-D
Heat Transfer/Fluid Flow/Electrochemistry	Electrolyzer	Concentration overpotentials from mixing correlations, Empirical ohmic resistance, 1-D	Concentration overpotentials from concentration gradient at electrode surface, Distributed ohmic resistance from material properties, 3-D
Heat Transfer/Fluid Flow/Chemical Reaction Kinetics	Chemical Reactor	Correlated rate constants, empirical reaction order, 1-D	Concentration dependence on space, Species diffusion, Boundary layer, Turbulence, 3-D

control volume. Piecewise profiles of the dependent variable are assumed between grid points. The profiles are integrated resulting in a discretization equation relating control volume averaged values of ϕ for a collection of grid points. The set of discretization equations for all grid points can be solved simultaneously when the values of the dependent variables at the border of the grid are given. When time rate of change appears as it does in the first term of Eq. (1), the space discretized equation is integrated from the start of the last solution time to the new solution time. When parameters Γ and S are constants the discretized equations are a set of linear equations in the dependent variables.

A.2. Solution

The above procedure will yield a set of algebraic equations that can in principle be solved for the dependent variables. But experience has shown several factors must be considered in developing a numerical scheme that will converge reliably to the correct solution.

Nonlinearities – The parameters Γ and S in Eq. (1) are in general functions of the dependent variables ϕ. Because of this nonlinearity the coefficients in what would otherwise be a set of linear discretized equations depend on the ϕ's. The solution procedure is this case is an iterative one where the values of ϕ are guessed at to provide initial fixed values for Γ and S and then the set of linear discretized equations is solved for the ϕ's. In an iterative fashion, these new values are used to update the estimate for Γ and S and the procedure is repeated until the change in the ϕ's from one iteration to the next satisfies a convergence criterion.

Donar Cell Defferencing - In deriving the discretized equations for a control volume the term $\rho u \phi$ appears at the faces of the control volume. However, since $\rho u \phi$ is defined only at the center of the control volume, a value must be interpolated from values of $\rho u \phi$ for adjacent volumes. It is known that a *donor-cell* expression rather than a *central-differenced* expression convergence more reliably. [3] In the donor-cell method, the control volume is regarded as a well-mixed tank while the upstream fluid is thought of as being delivered through a tube. In this scenario the upstream fluid is more decoupled from the control volume fluid and this tends to stabilize the numerical solution scheme.

Staggered Mesh - When the momentum equation grid overlays the grid for the mass and energy equations, artifacts in the velocity field can appear. By staggering the momentum equation grid relative to this second grid, these effects are eliminated. In this scheme velocity is defined at the center of the momentum control volume but because of the staggered mesh, these velocities are coincident with the faces of the mass and energy control volumes.

Fully Implicit Time - The time integral of the space discretized equation can be evaluated using a method where the integrand is a weighted average of the old and new time. When the weighting factor is unity only the integrand at the new time appears. The resulting time and space discretized equation is said to be fully implicit. All dependent variables appear at the new time with the exception the first term in Eq. (1) which is first order time differenced so that the dependent variable appears once at the old time step.

Under Relaxation – In the presence of strong non-linearities the change in a dependent variable from one iteration to the next may be large enough that an intermediate solution overshoots the true location of the solution causing the algorithm to diverge. For such cases the discretized equations can be modified such that the change in the dependent variable from one iteration to the next is limited by introduction of an *over relaxation* parameter. The solution to the discretized equation is not altered but the rate at which the dependent variable approaches the true value from iteration to iteration is reduced.

B. Ordinary Differential Equations

Under certain conditions the fundamental transport processes represented by the two terms on the right-hand side of Eq. (1) need not be modeled. In their place integral data derived from experiment (i.e. empirical) are used. As an example, for well-developed flow in a uniform channel, the overall behavior of the fluid measured in terms of heat transfer with the channel wall and pressure drop induced by shear at the wall correlates with several parameters. These are the average fluid conditions (temperature and velocity), fluid properties (viscosity and density), the wall conditions (temperature), and the channel characteristics (hydraulic diameter and surface roughness). Empirical data in the form of a heat transfer coefficient and friction factor provide the link between fluid and wall conditions. In such cases where only the integrated or average behavior is needed, then it is unnecessary to model the underlying transport processes.

B.1 Discretization

In the ODE approach regions of space are lumped such that only averaged values of dependent variables appear. A control volume encloses the lumped region and conservation balances are written for the volume. The exchange of mass, energy, and momentum between lumped regions is written in terms of a difference in temperature, pressure-velocity, or concentration between regions and then is multiplied by a heat transfer coefficient, friction factor, or diffusion coefficient, respectively. In essence the coupled spatially-discretized equations of the PDE are replaced by coupled algebraic equations in the lumped quantities. A time derivative remains and it is descretized in the same manner as for PDEs.

B.2 Solution

The issues associated with obtaining a solution parallel to a degree those for PDEs.
.
Nonlinearities - As in the case of the PDEs, the lumped parameter equations must be linearized with respect to the dependent variables before a solution can be obtained. Since the number of variables is a factor ten to thousands of times smaller, this linearization can be performed numerically, and rapid code execution still achieved. A standard approach is to compute the Jacobean matrix and use a descent method such as Newtons method to find the roots.

Flow Network - Similar to the staggered mesh used for the solution of PDEs a flow network represents how lumped regions communicate. The network consists of branches and nodes. A branch models mass (heat) flow in the momentum (energy) equation. A node represents pressure (temperature). Branches terminate at nodes at which point a mass (energy) balance is imposed.

For the transient case it follows that energy and mass storage and associated dependent variables are defined in the nodes while momentum inertia and associated dependent variables are defined in the braches. Hence, velocity is staggered with respect to energy. Figure 1 shows the conceptualization of flow in and around a VHTR fuel element while Figure 2 shows the unit flow network set up to solve for the flow in a two-dimensional array of these elements. This problem is from [4] where the performance degradation due to leakage around fuel elements was investigated. It is mentioned here only as an example of a flow network.

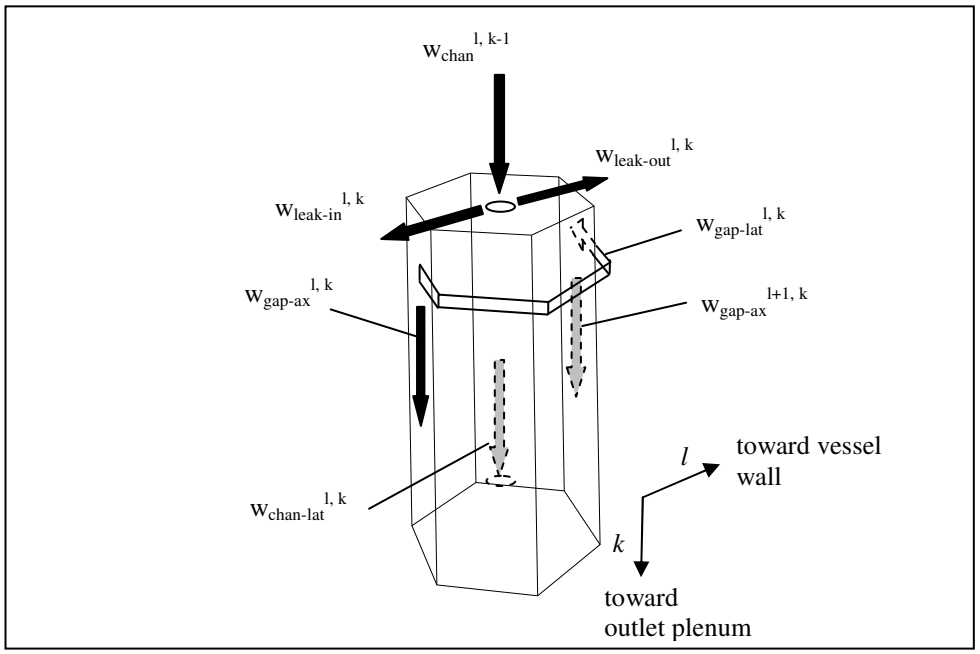

Fig. 1 Coolant Paths Through and Around an Element

Fully Implicit Time - The discussion for PDEs applies equally here.

Under Relaxation - The discussion for PDEs applies equally here.

Equation Scaling - Unlike solution schemes for PDEs, which alternate between solving for the flow field via the momentum equation and the temperature and density via energy and mass equations, all three equations are solved simultaneously. As a consequence large differences between equations in the magnitude of their terms will exist. Terms between equations may differ by a factor of 10^5 if temperature appears in Celsius in the energy equation and pressure in Pascals appears in the momentum equation. Large differences such as these can result in matrices that are poorly conditioned with the result that the solution scheme is less likely to converge. To guard against this, the equations should be scaled in advance. A method for automating the scaling of equations is described in [5].

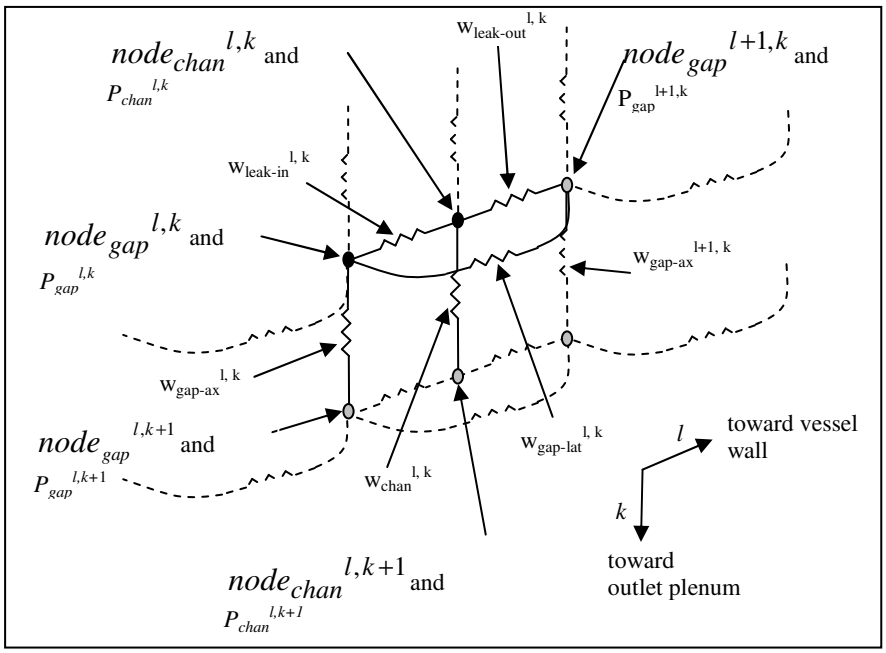

Fig. 2 Network Representation of Mass Nodes, Coolants Flowpaths, and Pressures. Unit network denoted by lines and nodes drawn in bold.

IV. FACTORS TO BE CONSIDERED IN CODE DEVELOPMENT

One purpose of this report is to present a review of methods for development of a dynamic simulation capability for system interface studies. The previous sections identified the phenomena basic to a good simulation and described both the lumped parameter and fundamental transport approaches to modeling. In this section we identify important code features and how they might be incorporated in light of the information already presented.

The steady-state case is marked by a large number of possible plant configurations that will be analyzed, many of them likely discarded in advance of the need for a dynamic analysis. The few configurations that do make it through for dynamic analysis will present the need for a large number of transient simulations. So while the steady-state case augers for a code that is modular for rapid assembly of many different equipment configurations, the dynamic case should place emphasis on development of a code that is fast running. A transient time step is roughly equivalent to solving for a steady-state solution. There will be a thousand time steps per second, and the average transient will evolve over tens of minutes. Transients will need to be simulated for various combinations of nuclear plant and hydrogen plant startup and shutdown, for various combinations of load changes, and for upset events. So if care is not exercised transient code execution time could conceivably be a bottleneck with respect to obtaining timely analysis results.

There are other considerations. The dynamic code should for reasons of practicality be an extension of the steady-state code. There will be data that is common to both codes that is best shared. This includes data associated with component models, plant configuration data, and a steady-state solution. Expanding on this, it is important to have consistency in models between the steady state and the transient, i.e. the non-storage terms that are solved in the steady state and that appear as non-dynamic terms in the dynamic equations. Ideally, these models should be identical. The transient code should use the same input scheme through which the user configures the equipment layout, otherwise the user will have to input data twice. Thus, significant advantage is to be had by having a transient code that is simply an extension of the steady-state code, essentially the steady-state code with dynamic terms added.

We summarize in light of what has been presented. It appears that a dynamic code that is modular in the sense the user can specify how components are connected (as has been implemented in the HyPEP code) and adopts lumped parameter models would best meet the needs of the project. The phenomena thought to be important can be adequately modeled using empirical data. The physical situations where transport of mass, energy, and momentum must be treated using fundamental models do not appear to arise in the transients of interest. Such models are needed for specialized cases that include shock waves in compressible fluids, multi-dimensional flow distributions in plena, radiation heat transport in complex geometries, multi-dimensional buoyancy-driven flow recirculation, explicit modeling of heat transfer and momentum transfer in the boundary layer, and high resolution tracking of coolant phase boundaries. None of the effects would appear to be important for the transients we identified for system interface studies. Essentially PDEs are needed in situations with non-uniform geometry that require fine spatial resolution for calculating fundamental transport processes because of lack of correlated data. The ODE approach on the other hand is suited for uniform geometries with processes that are primarily one-dimensional so that correlated integral data is readily available in the literature.

Another disincentive for the use of PDEs is long simulation run time. Run times comparable to codes used in nuclear safety analysis may be experienced. Transient runs will be measured in hours, and spatial resolution will be in excess of what is needed for system integration studies.

The numerical scheme should be fully implicit to the degree practical for good convergence behavior. This means that all dependent variables at the new time step are calculated simultaneously. In some situations there may be an incentive to be less than fully implicit. A particular component may require fine spatial nodalization (e.g. heat exchanger with large changes in coolant properties over space) and if so, the model could be converged locally in an inner iteration nested in the system wide iteration. This approach would provide the fine model detail when needed and can be implemented in a way that is consistent with the modular user-configurable approach.[5] It also serves to limit the size of the matrix equations that must be solved in the outer iteration and, hence, provides for faster execution. This approach may not be numerically well behaved, however, if there are interfaces that involve large property variations, as in the case of phase change, that must be tracked. But such cases arise only in detailed safety analyses and are not expected to appear in the systems interface work.

V. PRE-CODE ANALYSIS METHODS

A. Load Schedule

The dependence of process variables on the power level of the plant is given by the *load schedule*. Typically the plant load schedule is designed to maintain constant temperature at the hottest points in the plant (eg. reactor outlet) over all power while at load. What can be achieved from the standpoint of 1) the number of independently controllable actuators needed to achieve constant temperature at a given number of points and 2) the values actuator outputs need to assume to achieve a result is described below. One sees that a steady-state code equipped with the proper features can be used to determine the actuator properties needed to achieve a desired load schedule.

Each of the components in the plant in the steady state satisfies an equation of the form

$$0 = [\ y + F\ [\underline{u}(t)]\ ]$$

where

$\underline{u}(t)$	=	vector of input forcing functions,
F	=	function of $u(t)$,
y	=	component output.

Assume for the sake of exposition that there are three control variables: two flowrates, w_1 and w_2, and rod reactivity, ρ. Coupling the equations for all components leads to a system of equations for the plant state vector expressed in terms of the control variables

$$[T_1 T_2 ... T_n]^T = A_o(w_1, w_2, \rho\ )^{-1}\, b_o(w_1, w_2, \rho\ ) \qquad (2)$$

where the T_i are temperatures, A_o is a matrix whose elements are functions of the control variables, and b_o is a vector.

The control variables are written as linear functions of the plant power

$$w_1 = m_1 P + b_1$$
$$w_2 = m_2 P + b_2$$
$$\rho\ = m_3 (P - P_0)$$

where m_1, m_2, m_3, b_1, and b_2 are constants.

Differentiating the above set of equations with respect to power gives a set of load schedule coefficients that defines the load schedule about an operating point

$$\left[\frac{dT_1}{dP} \frac{dT_2}{dP} \bullet\bullet\bullet \frac{dT_n}{dP} \right]^T = A_1(m_1, m_2, m_3, T_1, T_2, ..., T_n)^{-1} b_1(m_1, m_2, m_3) \quad (3)$$

One sees from the above equation that three load coefficients can be arbitrarily assigned through the three parameters m_1, m_2, and m_3. This expression holds at a particular power. It can be applied repeatedly at different power to achieve the load schedule desired for three temperatures. In general, assigning values to n temperatures over the load range will require n actuators.

Building a capability for designing a load schedule using a dynamics code would involve assigning desired values for the process variables on the left-hand side of Eq. (2) at a given power and then solving for the unknowns on the right-hand side. This would be repeated for power over the normal at-load operating range.

B. Time Constants and Energy Capacitances

The combined plant response is shaped by the time constants of the various components. The time constants and where they appear in the flowpaths for the transport of the conserved quantities can provide insight into the time behavior of the overall plant.

The time response of a component is in the neighborhood of an operating point given by the ordinary differential equation

$$\frac{d}{dt} y = \frac{-1}{\tau} \left[y + F\left[u(t) \right] \right] \quad (4)$$

where $u(t)$ is the forcing function, y is the observed process variable, F is a function of u, and τ is the time constant. The role of the time constant is made evident by applying a step input to the component. The initial steady state satisfies from Eq. (4)

$$y\left(0^-\right) + F\left[u\left(0^-\right) \right] = 0 \ , \quad (5)$$

so the component response for a step in F applied at $t=0$ is

$$\frac{y(t) - y(\infty)}{y\left(0^-\right) - y(\infty)} = e^{\frac{-t}{\tau}}, \quad t > 0 \quad (6)$$

where $y(\infty)$ designates the new steady state. One sees that the observed variable moves to the new steady state with time constant τ.

Appendix A derives analytic expressions for time constants and energy capacitances for the major components in a coupled VHTR and HTE plant.

C. Load Change

The plant transient behavior is characterized by the response to a sudden change in demand. Examples of such changes are a step change in hydrogen or electricity demand. The time taken to come into equilibrium with the new demand condition, termed the *response time*, is important for meeting production goals and for safety-related integrity of structures.

Analyses based on component time constants and thermal capacitances can provide a measure of response time. Further, such analyses provide insight into what is controlling plant response and provide an adjunct to detailed transient simulation. The time constants and thermal capacitances control how long before the core and heat sink powers come back into equilibrium with each other after a change in conditions. A change in local conditions at the heat source (sink) flows through a series of processes each with a characteristic time constant before reaching the heat sink (source) where the temperature and flow changes create feedback effects that operate to bring all processes back to equilibrium. But until equilibrium is restored, a power generation imbalance gives rise to an energy imbalance approximated by

$$\delta E = \delta P \sum \tau_i \tag{7}$$

where δP is an initial step change in power and the τ_i are a series of process time constants through which the change must propagate before feedback effects occur to bring heat sink and core power back into equilibrium. The change in temperature caused by this power imbalance averaged among the i processes is

$$\delta T = \frac{\delta P \sum \tau_i}{\sum \left(\rho V C_p\right)_i} \tag{8}$$

If the original and terminal plant states are on the normal plant operating curve, as is the case for the instances we will look at, then the overshoot in temperature is given by

$$\delta T_{os} = \frac{\delta P \sum \tau_i}{\sum \left(\rho V C_p\right)_i} - \delta T_{load} \tag{9}$$

where δT_{load} is the change in temperature in going from the original to the new operating point on the plant operating curve. To make use of the above expression, one first needs to identify the propagation path for the transient and to calculate the time constant and thermal capacitances of the processes along the propagation path.

The rate of change in temperature before equilibrium is reached is from Eq. (8)

$$\frac{d\delta T}{dt} = \frac{\delta P}{\sum \left(\rho V C_p\right)_i} . \tag{10}$$

D. Stability

For safety reasons stability is an important aspect of nuclear plant design. A physical system is stable if the transition to a new state, as driven by altered forcing function values, is marked by a smooth and non-oscillatory transition. Stability can be qualitatively assessed by examining the system response to a step change in an input variable. Since a step is composed of an infinite set of frequencies it excites all modes of the system. The stability can also be assessed by more formal methods that examine eigenvalues of the system linearized about an operating point.[6] The physical processes that govern the response of the reactor to a change in the load is described and a simple expression that predicts how reactor stability trends with plant parameter values is given below.

There is a natural tendency for reactor power to follow a change in heat sink load. An increase in load reduces heat sink outlet temperature which propagates back to the reactor core to reduce inlet temperature, adding reactivity which increases power. The resulting core outlet temperature increase propagates back to the heat sink providing additional heat to meet the original increase in load. The potential for oscillations arises if the heat sink does not attenuate this returning temperature front. In this case the temperature front moves on to the core where it raises inlet temperature and causes reactor power to decrease. One sees that there is the potential for core power to alternately increase and decrease as the reactor inlet and outlet temperatures change out of phase with each other. The degree to which core power oscillations are dampened is a function of the attenuation of the temperature front at the heat sink and the size of the reactivity inlet temperature coefficient.

A simple reactivity balance shows how stability trends with integral reactivity parameters. The reactor power in the asymptote is related to the flowrate and inlet temperature through

$$0 = A\,(P - 1) + B\,(\frac{P}{W} - 1) + \mathrm{C}\,\delta T_i \tag{11}$$

as derived in Appendix A. The change in reactor outlet temperature expressed as a function of change in reactor inlet temperature is then

$$\delta T_{out} = \left(1 - \frac{C\,\Delta T_{c-100} / B}{\frac{A}{B} + 1} \right) \delta T_i \tag{12}$$

where A, B, and C are integral reactivity parameters, P and W are normalized power and flow, respectively, and δT_i is change in inlet temperature. If the expression within the parentheses is negative, then a change in inlet temperature in one direction leads to a change in outlet temperature in the opposite direction. Hence, to the extent the heat sink passes through without attenuation a primary hot leg temperature front associated with an increase in reactor power due to an initial reactivity addition, the reactor power will begin to decrease on negative temperature reactivity a time later equal to the propagation time around the primary system. For oscillations

to occur, this time must be long enough that the initial reactor power increase (due to the original reactivity addition) begins to equilibrate before the temperature front makes it back to the reactor. Thus, oscillations are favored if 1) the heat sink weakly attenuates primary hot leg temperature fronts, 2) the loop propagation time is more than a few tens of seconds (making it greater than the core time constant), and 3) the expression in parentheses in Eq. (12) is negative. The amplitude of these oscillations will increase as $C\Delta T_{c\text{-}100}/B$ becomes a larger positive number and A/B a smaller positive number provided the ratio of the two is more than unity.

VI. PRE-CODE ANALYSIS RESULTS

The methods of the previous section have been applied to characterize the dynamic response of the combined VHTR and HTE plant. The individual plants are shown in schematic form in Figures 3 and 4. The interface adopted for these two plants is the reference design identified in [1] and shown in Figure 5.

A. Time Constants and Energy Capacitances

Time constants and thermal capacitances for the major components in the combined VHTR/HTSE plant were estimated using the expressions in Appendix A. Values are summarized in Table II. They are used in the following subsections to draw some preliminary conclusions about dynamic response.

Some simple observations are made. The reactor and PCU vessel walls have very large thermal capacitances (1000 MJ/C) but the time constant for these components as they interact with the helium coolant is almost an hour. Thus, for upset events equilibrating over the order of several minutes, these capacitances will not be particularly active. However, during startup this capacitance will be important. It will not be important for operational transients since the vessel walls are maintained at constant temperature.

The overall time response of the contents of the reactor vessel is largely a function of the thermal-hydraulic characteristics of the fuel. The neutronics are essentially quasi-static compared to the fuel (3.7 s versus 9.5 s) while the fuel energy capacitance (200 MJ/C) is large. Based on the substantial fraction of reactor vessel space occupied by the fuel, this capacitance appears to be greater than all other structure capacitances with time constants smaller than a few tens of seconds. The helium coolant is insignificant (4.7 MJ/C) compared to the fuel.

In the HTE plant the energy capacitance of the electrolytic cells (270 MJ/C) is almost a factor of ten greater than all the other components combined (~30 MJ/C). The time constant (206 s) is also roughly ten times greater than the other components (12-35 s). As a consequence rapid transients (seconds) in the HTE plant will be muted in their impact on electrolytic cell temperature. Essentially, with the process heat components operating at a power level of 50 MWt small power transients (~5 MWt) will be limited in the rates of temperature change they can induce in the electrolytic cells (270 MJ/C energy capacitance). Similarly, with the electrolysis decomposition process depositing only about 10 MW of sensible heat in the cells, transients in

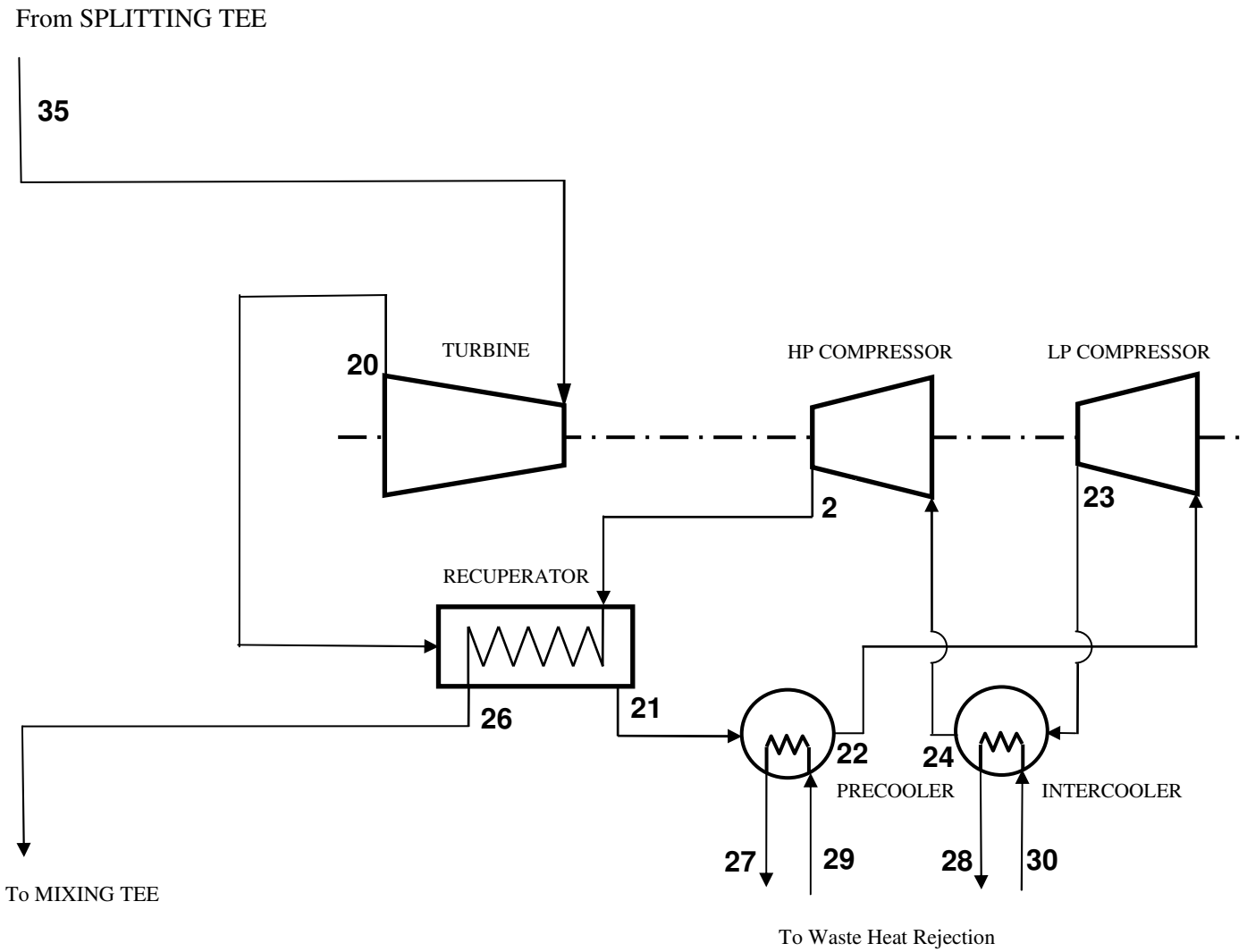

Figure 3 Network Diagram for PCU

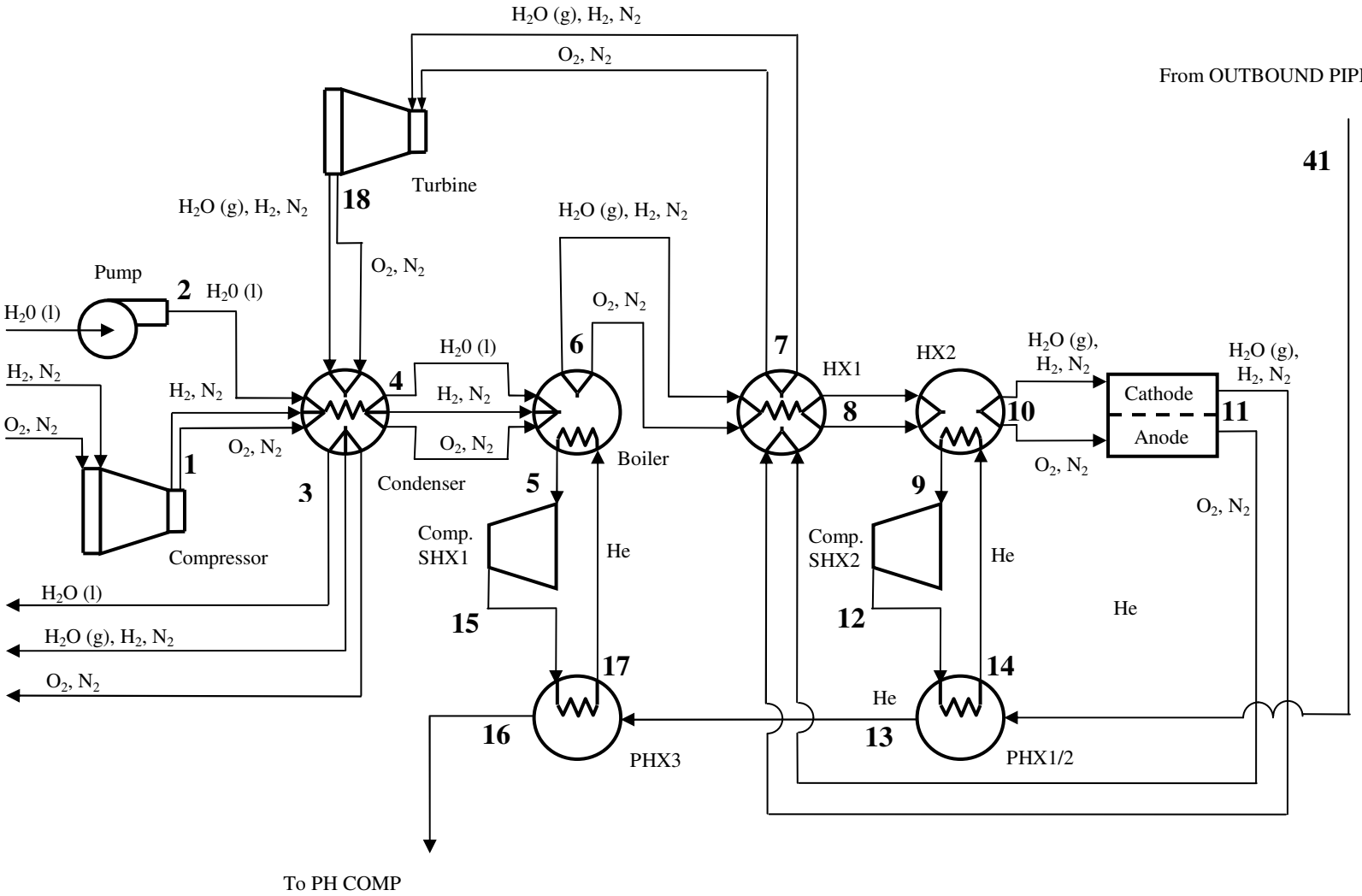

Figure 4 Network Diagram for HTE Process

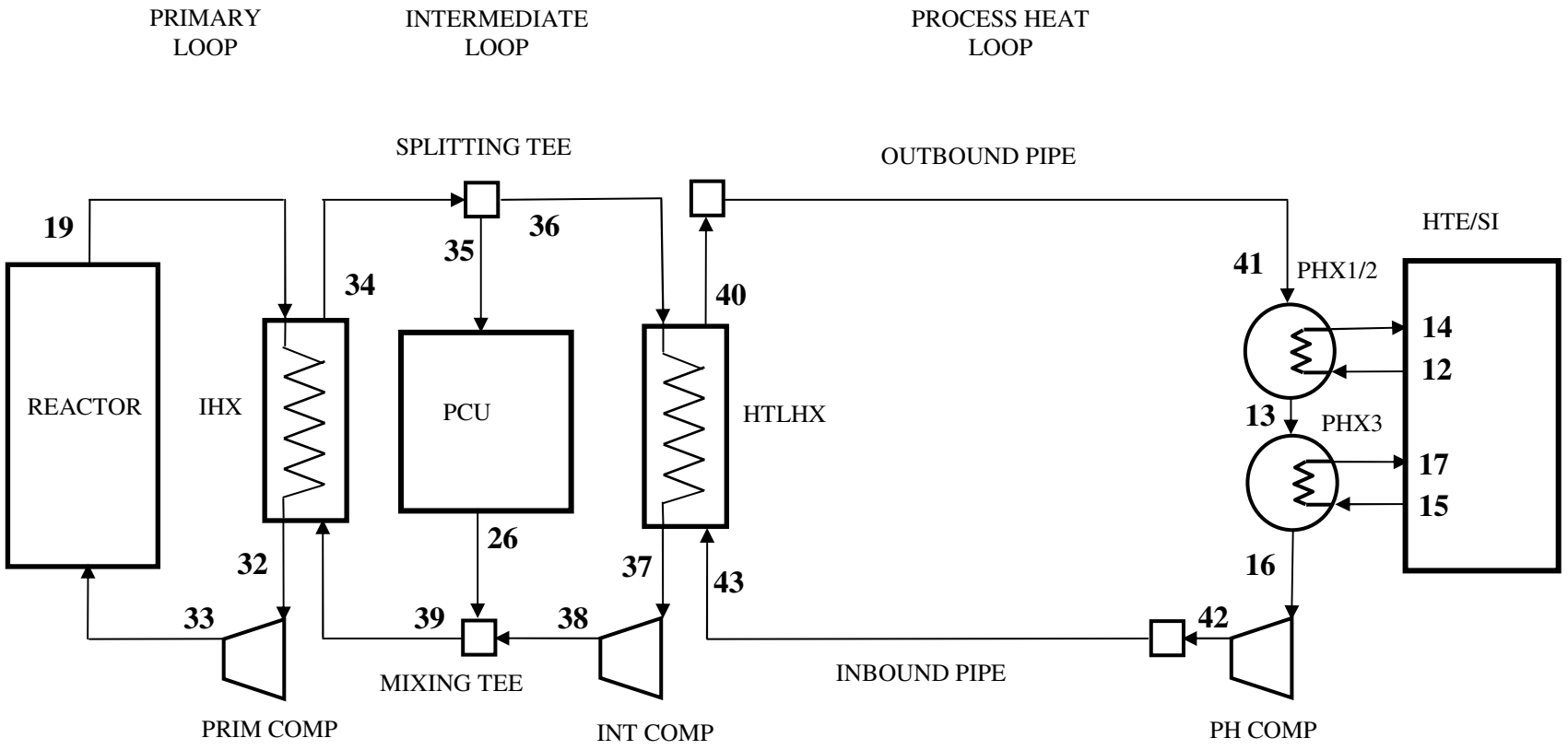

Figure 5 Network Diagram for Integrated System

Table II Summary of Thermal Time Constants and Capacitances

	Time Constant (s)	Energy Capacitance (MJ/^{o}C)	Ref.	Notes
Reactor Vessel				
Active Core				
Fuel Elements	9.5	200		
Neutronics	3.7	-		
He Coolant	2.8[a]	4.7		Assumes 0.2 void fraction
Internals	unknown	unknown		
Wall	4000	1000		< 500 C
Intermediate System				
IHX	0.28	27		
Flow Paths	unknown	unknown		
Power Conversion Unit				
Turbine	-	8.0[b]		
Recuperator	1.9	95		
Vessel Wall	2300	1000		< 500 C
Coolers	-	-		< 200 C
Compressors	-	-		< 200 C
HTE Plant				
HTLHX	0.96	2.8		
Outbound Pipe				
Pipe Wall	21	2.3		100 m; molten salt
Coolant	12	4.3		100 m; molten salt
Inbound Pipe				
Pipe Wall	21	2.3		100 m; molten salt
Coolant	12	4.3		100 m; molten salt
Condenser	30	7		
Boiler	20	2.3		
Superheater HX1	35	4.5		
Electrolytic Cells	206	270		

[a] Mixing [b] Based on mass of rotor and static structure estimated to be 16,000 kg

the electric generating part of the plant will result in limited rates of temperature change in the cells.

B. Load Change

A nuclear power plant connected to the electric grid has a normal at-load operating range of 25 to 100 percent of reactor full power. Below 25 percent power the generator is disconnected from the grid and the plant goes into standby mode with all reactor power dumped to the heat sink. For operation in the at-load power range, the plant load schedule gives the values of process

conditions (e.g. temperature) and control variables (e.g. pump flowrate or cooling circuit power removal). As described in Section V.A as the plant changes power quasi-statically, the control variables will change to according to the load schedule.

In addition to partial power steady-state operation, a power reactor is typically designed to be able to meet an instantaneous change in generator power of ten percent. The initial and final states are given by the load schedule. However, in the interim, dynamics are excited and the plant deviates from equilibrium. The transient behavior is obtained from a dynamic simulation. However, a measure of the deviation can be estimated using the method of Section V.C.

The load change considered is a ten percent step increase in hydrogen demand for the HTE plant of Figure 4. It is assumed that the reactants from Compressor 1and Pump 2 up to the Cell 11 inlet and the products from the Cell 1 output to Condenser 3 increase by this amount. All other flowrates in the combined plant and the electric power to the cell are assumed to remain constant. Of interest is the rate at which temperatures in the HTE plant change before the control system acts to bring control variables into agreement with the load schedule for the new hydrogen production level.

Inspection of Figure 4 reveals that the HTE equipment components containing either water and/or cell products are all tightly coupled thermally to each other. The two recuperating heat exchangers are responsible. An approximate estimate for the rate of temperature change throughout these components (condenser, boiler, HX1, HX2, cell, and turbine) is obtained from Eq. (10). Before the load change the thermal power provided by PHX1 and PHX2 is 50 MWt while the thermal output from the electrolyzer is about 10 MWt [7]. The energy capacitance from Table II is 270 MJ/C for the electrolyzer and about 30 MJ/C for the other components. The temperature rates of change amongst the components for a ten percent change in power will from Eq. (10) range from 0.02^{o} C/s (=0.1*60/300) to 0.17^{o} C/s (=0.1*50/30).

In summary, the rate of temperature change in each component will be limited to less than 0.2^{o} C/s. This is about a factor of five below rates (1^{o} C/s) that might lead to accumulated fatigue at the tube sheet in a large (hundreds of MW) tube and shell heat exchanger operating at 500^{o} C. The HTE heat exchangers are smaller (tens of MW) so temperature rates of change would have to be greater yet than 1^{o} C/s to create a fatigue problem. The exception may, however, be HX2 which operates at an outlet temperature of 850^{o} C.

C. Stability

General stability criteria for an at-power core coupled to a heat sink were developed in Section V.D. Essentially three criteria must be met, one of which relates the perturbation to core outlet temperature resulting from a temperature perturbation at the inlet. A necessary condition for the reactor to tend toward stable operation is that the core temperature feedback processes attenuate the effect of an inlet temperature perturbation on the outlet temperature of the core. Eq. (12) provides an expression for the degree of attenuation.

The magnitude and sign of the attenuation of inlet temperature perturbation was calculated for the VHTR core. The quantity in parenthesis in Eq. (12) was evaluated at full power conditions.

Table B-2 presents the estimate for rod differential worth. Normally the Operating Control Rods are inserted into the top of the core to maintain criticality. An increase in vessel temperature causes the rods to be move upward relative to the top of the core adding reactivity. An increase in fuel element temperature causes the core length to increase effectively causing the rods to move further into the core adding negative reactivity. The reactivity coefficients associated with these differential expansions are derived in Table III. The attenuation coefficient of Eq. (12) is calculated in Table IV. It has a value of -0.042 indicating near complete attenuation at the outlet of temperature perturbations arising at the inlet. On the basis of this one would expect the VHTR core coupled to a heat source to be very stable with respect to neutronic power.

Another stability assessment was made by comparing the values of two parameters identified in [6] as being important for controlling stability. These parameters and their values appear as the

Table III Deviation of Control Rod Reactivity Coefficients for VHTR

Operating Control Rods -Vessel	437·2.54e-2 =11.1
Length, L (m) (hot duct to top of core)	
Steel coefficient of thermal expansion, β (m/m/C)	1.5e-5
Differential worth, dρ/dL ($/m) [Table B-2]	3.1
$\alpha_{cr\text{-}v}$ [Eq. (A-3)] ($/°C)	11.1·1.5e-5 ·3.1 = 5.2e-4
Operating Control Rods - Moderator	7.93
Length[a], L (m) (active core height),	
Graphite coefficient of thermal expansion, β (m/m/C)	0.3e-5
Differential worth, dρ/dL ($/m) [Table B-2]	3.1
$\alpha_{cr\text{-}m}$ [Eq. (A-3)] ($/°C)	-7.93·0.3e-5 ·3.1 = -0.74e-4

[a] p.30 of [15]

Table IV Integral Reactivity Coefficients for VHTR

Operating Control Rods - Vessel, $\alpha_{cr\text{-}v}$ ($/°C)	[0,+5.2e-4][a], mean=2.6e-04
Operating Control Rods - Moderator, $\alpha_{cr\text{-}m}$ ($/°C)	-0.74e-4
Moderator, α_m (dk/dT) @ 770° C [b] (Fig. 37 [15])	[-1.0e-5, +4.0e-5]
α_m ($/°C)	[-1.67e-3, +6.67e-3], mean=2.5e-03
Fuel, α_f (dk/dT) @ 820° C [b] (Fig. 35 [15])	[-5.5e-5, -4.4e-5]
α_f ($/°C)	[-9.2e-3, -7.3e-3], mean= - 8.25e-03
Average moderator temperature rise[b], $\Delta T_{m\text{-}100}$ (°C)	100
Average fuel temperature rise[b], $\Delta T_{f\text{-}100}$ (°C)	50
Coolant temperature rise, $\Delta T_{c\text{-}100}$ (°C)	510
$A = \alpha_f \ (\Delta T_{m\text{-}100} + \Delta T_{f\text{-}100})$, ($)	- 1.2
$B = (\alpha_m + \alpha_{cr\text{-}m} + \alpha_f)/2 * \Delta T_{c\text{-}100}$, ($)	- 1.5 [d]
$C = \alpha_{cr\text{-}v} + \alpha_m + \alpha_{cr\text{-}m} + \alpha_f$	-5.6e-03 [d]
A+B, ($)	- 2.7 [d]
$1 - \frac{C\Delta T_{c-100}/B}{\frac{A}{B}+1}$	- 0.042 [d]
$C\Delta T_{c-100}/B$	0.90 [d]
$\frac{A}{B}$	0.83 [d]

[a]Vessel time constant is large at six inch thickness. Range covers time that varies from instantaneous to infinite.
[b]Average moderator and fuel temperatures from Table 11 of [15].
[c]β_{eff} ~$6x10^{-3}$.
[d] based on mean values

last two entries in Table IV. Figure 6 shows these values plotted on a stability map taken from [6]. According to this map the core power again is stable with respect to coupling to a heat sink. Note that in Figure 6 the x and y axis parameters are the same as the second last and last entries, respectively, in Table IV.

These stability criteria are probably of greater significance for coupling to the Sulfur Iodine (SI) plant compared to the HTE plant. Consider first the case of the HTE plant. More than 90 percent of the VHTR core thermal power is delivered to the PCU. The coupled neutronic and thermal feedback processes in the core have a combined time constant of about 10 s (Table II) while the transit time from the core outlet through the IHX and through the turbine and recuperator of the PCU and back to the core inlet is estimated to be about 10 s based on an estimated helium volume of 700 m^3 and a mass flowrate of 320 kg/s. This comparatively short transit time means the opportunity for out of phase behavior is minimized. While the thermal power delivered to the HTE plant has a propagation time through the outbound and inbound pipes of the order 25 s (Table II) and thus would tend to promote oscillations, the power is only a few percent of the total core power. Hence, the reactor inlet temperature perturbation introduced through this path will be small and not a strong source of instability. Next consider the SI plant. This heat sink consumes almost all the core thermal power while the propagation time through the outbound and inbound pipes to the hydrogen plant cited above is significantly longer than the 10 s core

time constant. Thus, stability issues will be more pronounced for the VHTR coupled to the SI process compared to the HTE process.

Future work should examine the more general case of reduced primary flowrate to characterize how attenuation represented by Eq. (12) is changed. The transit time through the PCU will increase to a value that exceeds the core power time constant violating one of the three stability criteria.

D. Startup

A preliminary procedure for bringing the combined plant up to full power from cold subcritical is given in Table V.

The time taken to reach full power is limited by the reactor power input to the combined plant and the heat capacity of the combined plant. Table II suggests that the total heat capacity is of the order 3000 MJ/C. Suppose the reactor power is raised linearly from 0 to 600 MWt and half of the heat is rejected to the heat sink. If the plant is at room temperature and on average is raised to the core mid-plane temperature at full power, then the time taken is

$$3000E06(J/C) * 700 (C) / (600E6(J/s) * 0.5 * 0.5) = 14{,}000 \text{ s}$$

or about four hours.

However, the time rate of change of temperature in thick structures such as the wall of the reactor and PCU vessels may have to be limited to achieve acceptable thermal stresses. There may be a similar consideration for the pressure boundary for the electrolytic cells which operate at high temperature and pressure. Thus, a startup time of four hours is a lower bound.

E. Reactor Trip

A reactor trip would be followed by an automatic runback in primary flowrate to avoid thermal shocking primary system hot side components, the IHX, and PCU components. The generator would automatically disconnect from the grid since it would not be able to meet grid demand. The result is that the electrical power to the electrolyzer and the thermal power to the HTE plant would drop to near zero. In the scenario envisioned the molten salt line to the HTE plant would no longer be heated but would still be in thermal contact with the boiler water inventory. Unless isolated, the water would continue to boil draining heat from the lines possibly causing the salt to freeze.

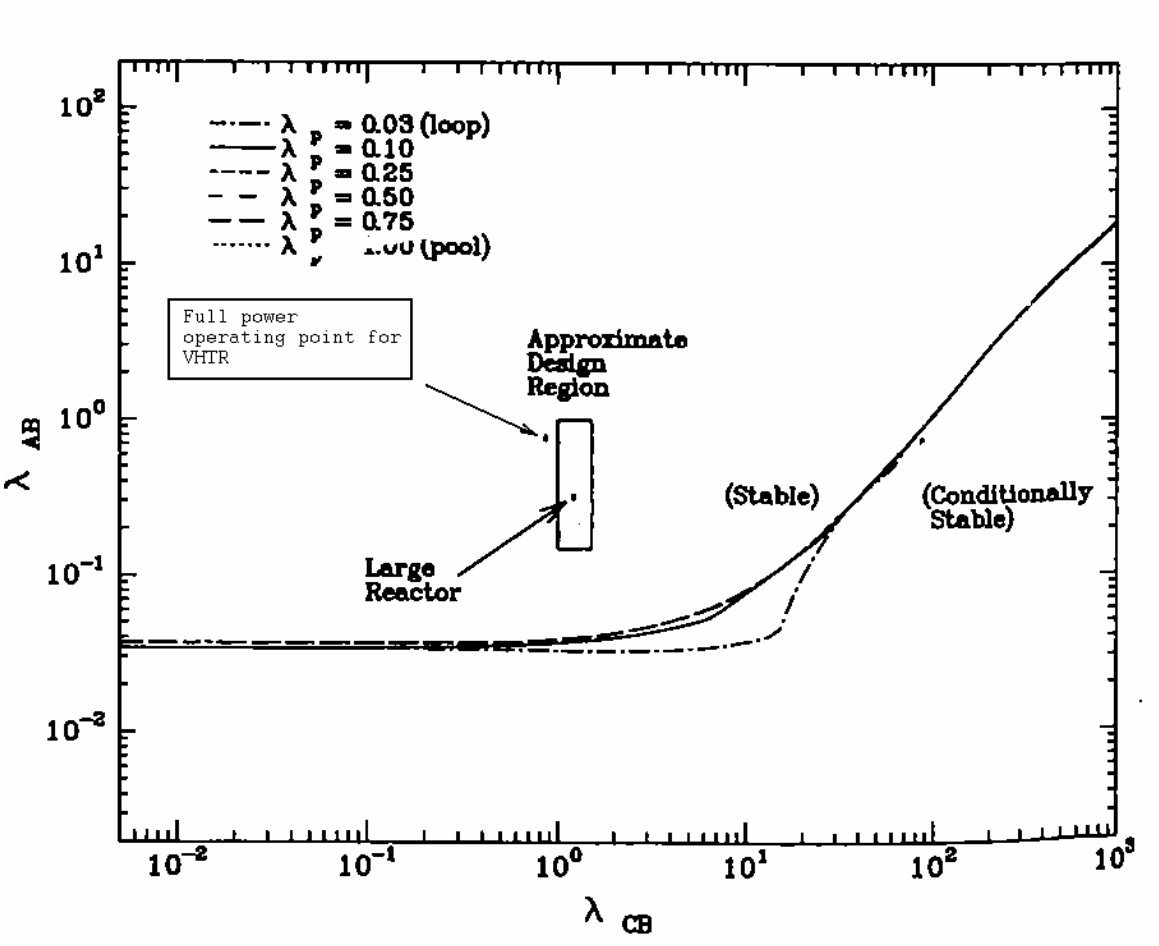

Figure 6 Location of VHTR at Full Power on Coupled Neutronic-Thermal Hydraulic Stability Map at Full Power Condition (adapted from [6])

The issue is how much margin to freezing would remain if the boiler were not isolated? A simple calculation provides some insight. For the boiler volume computed from data in Tables B-9 and B-10 and an assumed void fraction of 0.667, the resulting inventory is capable of removing approximately 300 MJ of energy through the latent heat of vaporization. Based on an initial sizing of the boiler the latent heat of vaporization of the water inventory is approximately 300 MJ. (Note this differs from the value in Table II which applies only about an operating point.) Table II shows the molten salt lines represent about 14 MJ/C of heat capacity. Thus, the water inventory could lower the average temperature of the molten salt lines by about 20^{o} C, probably not enough to freeze all the salt. Depending on the nature of the gravity head in the molten salt line, local freezing near the boiler might be averted by maintaining natural circulation in the molten salt circuit with the boiler acting as a heat sink.

VII. CONCLUSIONS

Some preliminary conclusions are drawn for the case of the VHTR coupled to the HTE process. In assessing the stability of the coupled plant it was found that the core outlet temperature response remains essentially unchanged with respect to inlet temperature perturbations suggesting the VHTR tends toward stable operation when coupled to a heat sink such as a hydrogen plant. In estimating the time required to start up the combined plant, on heat capacity considerations alone and assuming a linear ramp up of reactor power, full power conditions starting from cold shutdown can be reached in four hours. This is within the typical startup time of 24 hours for a nuclear plant. In the analysis there was no consideration given for exceeding limiting thermal stresses, however. In assessing temperature rates of change during load change, it was found that a ten percent step change in hydrogen production rate would result in a maximum average rate of change in temperature in the hydrogen plant of less than 0.2 C/s before the control system began to re-establish equilibrium with the rest of the combined plant. Given the relatively small size of the components in the HTE plant and, hence, a small wall and tube sheet thickness, this rate of change does not appear to present a thermal fatigue problem. Finally, it was found that a reactor trip followed by failure to thermally isolate the HTE boiler from the molten salt process heat loop coming from the reactor could lower the temperature of the salt by as much as 20 C. The issue is to avoid freezing the salt. Given that there might be a couple of hundred degrees margin between the coldest point in the loop and the salt freezing temperature no large-scale freezing appears possible. Whether local freezing occurs would depend on the natural circulation characteristics of the molten salt loop.

Table V Preliminary Startup Procedure for Representative VHTR/HTE Plant Configuration

Combined Plant Operating Mode	Sequence of Control Actions	Terminal condition
Reactor to Hot Critical	-	Subcritical core, cold and atmospheric pressure primary system
	Add inventory	Subcritical core, cold and uniform partially pressurized primary system
	Turning gear on	Subcritical core, hot and non-uniform partially pressurized primary system
	Add rod reactivity	Critical core, hot and non-uniform partially pressurized primary system
Ascend to House Electric Load	Add rod reactivity, turn on coolers, decouple turning gear	Plant self-sustaining as a heat engine
	Add rod reactivity	Increase turbomachine speed to match grid frequency
	Synchronize to grid and raise power to equal house load	Reactor at about 3 % load
	Turn on molten salt heaters	Thawed hydrogen plant heat transport loop
Ascend to House Thermal Load	Startup PH and SHX1 compressors	Two-phase region in boiler
	Increase reactor power, increase flow of PH and SHX1 compressors, turn on water pump	Saturated steam delivered to electrolyzer
Ascend to Bottom of Operating Range	Startup SHX2 compressor	Superheated steam delivered to electrolyzer
	Increase reactor power. Deliver electric power to electrolyzer.	Electrolyzer at temperature at bottom of operating range
Ascend to Full Power	Follow combined plant load schedule to full power condition: Inventory Control for reactor, Flowrate Control for HTE plant	HTE plant at full power hydrogen production

VIII. REFERENCES

1. C. H. Oh *et al.*, "HyPEP FY06 Report: Models and Methods," INL/EXT-06-11725, 2006.

2. B. Boyack, et al., *Quantifying Reactor Safety Margins, Application of Code Scaling, Applicability, and Uncertainty Evaluation Methodology to Large-Break, Loss-of-Coolant Accident*, NUREG/CR-5249, Nuclear Regulatory Commission, December 1989.

3. S. V. Patankar, "Numerical Heat Transfer and Fluid Flow," Hemisphere Publishing, 1980.

4. R.B. Vilim, "GAS-NET: A Two-Dimensional Network Code for Prediction of Core Flow and Temperature Distribution in the Prismatic Gas Reactor," ICAPP 2007 International Congress on Advances in Nuclear Power, Nice, France, May 13-18, 2007.

5. N. Carstens, "Control Studies for Supercritical Carbon Dioxide Power Conversion Systems," Ph.D. thesis, Department of Nuclear Engineering, Massachusetts Institute of Technology, June 2007.

6. E.V. Depiante, "Stability analysis of a liquid-metal reactor and its primary heat transport system," Nuclear Engineering and Design, 152, pp.261-377, 1994.

7. R.B. Vilim, Argonne National Laboratory, private communication, October 2006.

8. C. Oh., personal communication, Idaho National laboratory, November 2006.

9. R. B. Vilim, "Transient Response of a Natural Circulating Liquid-Metal Reactor from Time Constants and Energy Capacitances," Monitoring and Control Technologies for the Secure, Transportable, Autonomous Reactor (STAR), Nuclear Energy Research Initiative Field Work Proposal 24441, September 2001.

10. J. Hartvigsen, personal communication, Ceramatec, November 28, 2006.

11. S. Pradhan, *et al*., "Effects of Electrical Feedbacks on Planar Solid-Oxide Fuel Cells," ASME Transactions on Fuel Cell Science and Technologies, vol. 3, issue 4, November 2006.

12. T. Ohta, "Solar-Hydrogen Energy Systems," Pergamon Press, 1979.

13. Gas Turbine-Modular Helium Reactor (GT-MHR) Conceptual Design Report, Report number 910720/1, General Atomics, July 1996.

14. T. M. Lillo *et al*., "Engineering Analysis of Intermediate Loop and Process Heat Exchanger Requirements to Include Configuration Analysis and Materials Needs," INL/EXT-05-00690, September 2005.

15. P. MacDonald, "NGNP Point Design – Results of the Initial Neutronics and Thermal-Hydraulics Assessments during FY-03," INEEL/EXT-03-00870 Ref. 1, September 2003.

APPENDIX A ODE LUMPED PARAMETER COMPONENT MODELS

Expressions for the time constant and energy capacitance of a component are obtained by writing lumped parameter ODEs and then linearizing. The ODEs are derived from conservation balances and can be solved numerically to obtain a time dependent solution. Linearization is performed for the sole purpose of obtaining an expression for the time constant.

A.1 Reactor Neutronics and Heat Transfer

The natural time constant of the neutronic power depends on the reactivity associated with temperature feedbacks as shown shortly.This reactivity is expressed as a sum of individual reactivities. A reference state is defined and with it individual component temperatures. For convenience this state is taken as the full power steady-state condition. With respect to this state the reactivity introduced by a change in temperature of a component is given by

$$\rho = \frac{d\rho}{dL} L \beta \delta T \tag{A-1}$$

where is L is length, β is the coefficient of linear expansion, and δT is the temperature change. Of course, the individual component reactivities are dependent on the arrangement of components within the reactor vessel. We develop these for the GT-MHR upon which the VHTR is based. For this particular design 1) the reactor inlet coolant enters the core at the top and flows vertically down, 2) the control rod drive mechanisms are fixed to the top of the vessel and the rods enter at the top of the core, 3) the core rests on the bottom of the vessel, 4) the vessel wall is cooled by the coolant entering the reactor vessel, 5) the physical dimensions of the core are large compared to the neutron mean free path such that reactivity chage associated with a change in leakage due to core temperature expansion is insignificant, and 6) the reactivity feedback associated with coolant density is negligable.

Temperature changes in the core introduce control rod reactivity in two ways. First, the vessel temperature is assumed equal to the reactor inlet temperature so the vessel length changes in response to reactor inlet temperature resulting a change in control rod position relative to the top of the core. Second, the temperature of the graphite moderator blocks are assumed equal to the coolant temperature so the core length changes in response to the coolant temperature resulting in a change in control rod position relative to the top of the core. The net change in reactivity is then given by

$$\delta \rho = (-(L \beta)_v \delta T_i + (L \beta)_m \delta T_m) \left(\frac{d\rho}{dL} \right)_{cr} \tag{A-2}$$

where

T_i = reactor inlet coolant temperature and
T_m = reactor midplane moderator temperature, and

where the last term is the change in reactivity per unit change in the position of the rods with respect to the top of the core. Insertion into the core is taken as the positive direction. The

subscripts *v*, *m*, *cr* represent vessel, moderator, and control rod, respectively. The above expression is rewritten as

$$\delta\rho = \alpha_{cr-v}\,\delta T_i + \alpha_{cr-m}\,\delta T_m \tag{A-3}$$

where $\alpha_{cr-v} = -(L\beta)_v \left(\frac{d\rho}{dL}\right)_{cr}$ and $\alpha_{cr-m} = (L\beta)_m \left(\frac{d\rho}{dL}\right)_{cr}$.

The total change in reactivity due to temperature change is the sum of that associated with the control rods, the moderator, and the fuel and is given by

$$\delta\rho = \alpha_{cr-v}\,\delta T_i + \alpha_m\,\delta T_m + \alpha_{cr-m}\,\delta T_m + \alpha_f\,\delta T_f \tag{A-4}$$

where

T_m = average moderator temperature.

Note that the moderator and fuel temperature changes are related to the reactor power-to-flow ratio and the reactor power through the expressions,

$$\delta T_m = \delta T_i + \frac{\Delta T_{c-100}}{2}\left(\frac{P}{W} - 1\right) + \Delta T_{m-100}(P-1), \tag{A-5}$$

$$\delta T_f = \delta T_i + \frac{\Delta T_{c-100}}{2}\left(\frac{P}{W} - 1\right) + (\Delta T_{m-100} + \Delta T_{f-100})\,(P-1)\,, \tag{A-6}$$

where

P = fission plus decay power normalized to full power condition,
W = flowrate normalized to full power condition,
$\Delta T_{c\text{-}100}$ = mixed mean reactor coolant temperature rise at full power condition,
$\Delta T_{m\text{-}100}$ = average moderator temperature rise at full power condition, and,
$\Delta T_{f\text{-}100}$ = average fuel temperature rise at full power condition.

If the feedback components in Eq. (A-4) are linear, then substituting the above expressions into Eq. (A-4) and collecting terms gives

$$\rho = (\alpha_{cr-v} + \alpha_m + \alpha_{cr-m} + \alpha_f)\,\delta T_i + (\alpha_m + \alpha_{cr-m} + \alpha_f)\frac{\Delta T_{c-100}}{2}\left(\frac{P}{W} - 1\right) + \alpha_f\,(\Delta T_{m-100} + \Delta T_{f-100})\,(P-1) \tag{A-7}$$

or

$$\delta\rho = A(P-1) + B\left(\frac{P}{W}-1\right) + C\,\delta T_i \tag{A-8}$$

where

$$A = \alpha_f\,(\Delta T_{m-100} + \Delta T_{f-100}) \tag{A-9}$$

$$B = (\alpha_m + \alpha_{cr-m} + \alpha_f)\frac{\Delta T_{c-100}}{2}\ ,$$

$$C = \alpha_{cr-v} + \alpha_m + \alpha_{cr-m} + \alpha_f\ .$$

For the transients of interest the reactivity is always much less than β so that the prompt jump approximation can be made. If also the number of precursor groups is taken as one, then the normalized fission power is given by

$$\left[\rho(t)-1\right]\frac{dP}{dt} + \left[\lambda_f \rho(t) + \frac{d\rho}{dt}\right]P(t) = 0\ . \tag{A-11}$$

where the reactivity has been normalized to β and has units of dollars. The above equation is rearranged as

$$\frac{d}{dt}P = \frac{1}{\tau}P \tag{A-12}$$

and has solution

$$P = Ke^{t/\tau} \tag{A-13}$$

where

$$\tau = \frac{1-\rho}{\lambda\rho + \frac{d}{dt}\rho}\ . \tag{A-14}$$

The solution reveals the neutron population response has characteristic short and long term behavior. For a near step change in reactivity, in the short term as the reactivity is being added

$$\tau \approx \left(\frac{d}{dt}\rho\right)^{-1}\ . \tag{A-15}$$

Once the near step reactivity has been added, assuming $\rho << 1$, then

$$\tau \approx \frac{1}{\lambda\rho} . \tag{A-16}$$

which shows the approach to equilibrium proceeds initially with a time constant longer than that of the delayed neutron time constant followed by a continual lengthening.

An expression for the time constant of the core power when reactivity enters through reactivity feedbacks is obtained as follows. The reactivity is given by

$$\rho = A\left(P-1\right) + B\left(\frac{P}{W}-1\right) + C\delta T_{i} + \rho_{rod} \tag{A-17}$$

where the power, P, and flowrate, W, are normalized to some equilibrium condition. Here we have assumed that the core temperatures remain in equilibrium as power and flow change (in fact they will lag according to the thermal time constants of the structures that provide the reactivity feedback). From Eq. (A-12) and (A-16), if we let $P=1+\delta P$, $W=1+\delta W$, and drop other than first-order terms, then the power is given by

$$\frac{d}{dP}\delta P = \frac{1}{\tau}\delta P + \lambda\left[-B\delta W + C\delta T_{i} + \rho_{ext}\right], \quad \tau = \frac{-1}{\lambda\left(A+B\right)} . \tag{A-18}$$

The power change related to reactivity insertion is denerated in the fuel kernels and must flow through the fuel element matrix material and into the coolant before equilibrium is attained. There is a time constant and energy capacitance associated with the matrix material. Expressions for these are obtained by representing a unit cell of the matrix of coolant, moderator, and fuel as a solid cylinder with fuel and moderator smeared homogeneously and in contact with the coolant at its outer surface. In general it is not possible to preserve mass and heat transfer area simultaneously. In Appendix B.1, mass is preserved.

The one-dimensional lumped-parameter temperature response of a cylinder to a change in internal heat generation rate or applied surface temperature is

$$\frac{d}{dt}T = \frac{-1}{\tau}\left[T + F\left(t\right)\right], \qquad \tau = \frac{\rho V C_{p}}{2\pi r\ hL} \tag{A-19}$$

where

$$\frac{1}{h} = \frac{r}{4k} + \frac{1}{h_{c}} . \tag{A-20}$$

In the above expression the first term is material conduction resistance and the second term is contact resistance.

A.2 Heat Exchanger

The efficiency of the closed Brayton cycle is very sensitive to pressure losses and so there is an incentive to use heat exchangers with a high effectiveness/low pressure drop characteristics. Generally, this implies plate and fin or printed circuit heat exchangers (PCHE) in a counter flow configuration. This section develops models for the PCHE which seem to be preferred in recent design studies.

The construction of a typical PCHE is shown in Figure A-1. The design consists of alternating hot and cold plates with semi-circular parallel flow channels etched into the lower face of each plate with the channels carrying the respective hot and cold streams. The hot and cold streams flow in opposite directions.

The energy equation for the hot side coolant node is

$$V\frac{d(\rho h)_{h_o}}{dt} = -Q_{h-t} + w_{h_i}h(T,P)_{h_i} - w_{h_o}h(T,P)_{h_o} \tag{A-21}$$

where $Q_{h\text{-}t}$ is the rate of total heat transfer from the hot side coolant to the heat transfer media which we refer to as a tube and h is enthalpy. Similarly, the energy equation for the cold side coolant is

$$V\frac{d(\rho h)_{c_o}}{dt} = Q_{t-c} + w_{c_i}h(T,P)_{c_i} - w_{c_o}h(T,P)_{c_o} \tag{A-22}$$

where $Q_{t\text{-}c}$ is the rate of total heat transfer from the tube to the cold side coolant. The energy equation for the tube is

$$V\frac{d(\rho C_p T)_t}{dt} = -Q_{t-c} + Q_{h-t}. \tag{A-23}$$

In the case where the tube metal is lumped with one of the coolants rather than solving separately for its temperature, the heat transfer rate from hot to cold fluid is for constant fluid properties

$$Q = AU\frac{(T_{ho}-T_{ci})-(T_{hi}-T_{co})}{\ln((T_{ho}-T_{ci})/(T_{hi}-T_{co}))}. \tag{A-24}$$

A unit cell, defined as a region delineated by four boundaries across each of which there is zero net energy flow, for characterizing the different heat transfer processes. Figure A-2 shows two adjacent unit cells contained in the cross section of an infinite array of alternating hot and cold plates. We consider the upper unit cell in Figure A-2. Both unit cells are similar enough that this one suffices for obtaining representative time constants. Heat flows from the hot channel on the bottom to the cold channel on the top. The dashed horizontal lines drawn through each channel identify cell boundaries across which there is not net flow of energy. Of course, the energy flow

in the cell shown is two dimensional and it is assumed this distribution is known so that the cell boundaries can be drawn as the dashed lines shown. This establishes dimension *t'* shown in the figure.

A one-dimensional representation of heat flow between the channels in the top unit cell is shown in Figure A-2. This is of course an approximation to a multidimensional heat flow problem but captures to the first order the energy storage mechanisms and heat flow resistances of the three regions: the hot channel, the cold channel, and the intervening heat transfer media. The coolant in the channels that interacts with the heat transfer media in the cell is marked by the hash lines in the channels. This fluid has a cross sectional area denoted by A and it makes contact with the media through circumference C. The circumference is the solid line that abuts the hash lines. The hot stream, media, and cold stream have average temperatures T_h, T_m, and T_c, respectively, shown in Figure A-2. The heat transfer between the hot stream and the media is approximated by

$$T_h - T_1 = \frac{Q/l}{C_h h_h} \tag{A-25}$$

where T_1 is the temperature at the surface of the media in contact with the hot stream, h_h is the heat transfer coefficient between the hot stream and the surface of the media, and k is the thermal conductivity of the media. Similarly, the heat transfer through the media is approximated by

$$T_1 - T_m = \frac{Q/l}{\frac{k\,P}{t/2}\,\frac{(t/2*P - A_h)}{t/2*P}} \tag{A-26}$$

where A_h is the hot fluid cross sectional area of the unit cell. The factor on the right in the denominator attempts to correct for the reduction in the cross section of the media caused by the hot channel and its subsequent effect on average conductivity. Alternatively, this correction factor could be obtained from the solution to the two-dimensional conduction equation for the media. The above two equations yield

$$Q = \bar{h}_{h-m}\, l\, (T_h - T_m) \tag{A-27}$$

where

$$\bar{h}_{h-m} = \left(\frac{1}{C_h h_h} + \frac{1}{\frac{k\,P}{t/2}\,\frac{(t/2*P - A_h)}{t/2*P}} \right)^{-1} . \tag{A-28}$$

Similarly, the heat flow between the media and the cold channel is given by

$$Q = \bar{h}_{m-c}\, l\, (T_m - T_c) \tag{A-29}$$

where

$$\bar{h}_{m-c} = \left(\frac{1}{C_c h_c} + \frac{1}{\frac{k\,P}{t/2}\,\frac{(t/2*P - A_c)}{t/2*P}} \right)^{-1} \quad . \tag{A-30}$$

An energy balance on the hot channel coolant in thermal contact with media over a length l gives

$$(\rho A\, l C_v)_h \frac{dT_h}{dt} = -(C_p w)_h (T_h - T_i) - \bar{h}_{h-m}\, l\, (T_h - T_m) \tag{A-31}$$

where ρ is density, C_p is specific heat, w is flow rate, and subscript i refers to inlet. Similarly, for the media

$$(\rho A\, l C_p)_m \frac{dT_m}{dt} = -\bar{h}_{h-m}\, l\, (T_m - T_h) - \bar{h}_{m-c}\, l\, (T_m - T_c). \tag{A-32}$$

Rewriting these two equations in terms of time constants,

$$\frac{dT_h}{dt} = -\frac{1}{\tau_{i-h}}(T_h - T_i) - \frac{1}{\tau_{h-m}}(T_h - T_m) \tag{A-33}$$

and

$$\frac{dT_m}{dt} = -\frac{1}{\tau_{m-h}}(T_m - T_h) - \frac{1}{\tau_{m-c}}(T_m - T_c) \tag{A-34}$$

where

$$\tau_{i-h} = \frac{(\rho A\, l\, C_v)_h}{(C_p w)_h}, \qquad \tau_{h-m} = \frac{(\rho A\, C_v)_h}{\bar{h}_{h-m}}, \qquad \text{and} \tag{A-35}$$

$$\tau_{m-h} = \frac{(\rho A\, C_p)_m}{\bar{h}_{h-m}}, \qquad \tau_{m-c} = \frac{(\rho A\, C_p)_m}{\bar{h}_{m-c}}. \tag{A-36}$$

Three nodes representing the hot side coolant, heat transfer media, and cold side coolant. A lumped parameter energy storage equation is written for each of the nodes. When writing these equations it is assumed from the standpoint of energy storage that there is perfect mixing of the energy that enters a node so that the node is at a uniform temperature.

General expressions are developed for the parameters C_h, A_h, C_c, and A_c that appear above. The location of the zero heat flow boundaries in Figure A-2 is referenced in terms of the displacement t'. In the absence of a solution to the two-dimensional conduction equation, we

assume the zero net heat flow line is located where one-half of the channel perimeter lies above the line and the other half below. The total channel perimeter is *r*(π+2).* Let the angle between the base of the semi-circle and the radius that intersects the zero heat flow line be θ. Then θ satisfies

$$\frac{1}{2}C = \frac{1}{2}r(\pi+2) = 2r + 2r\theta \quad \text{or} \qquad \theta = \frac{1}{4}(\pi-2) \tag{A-37}$$

where C is the total perimeter of the channel. We have then for the hot channel in the unit cell (i.e. hashed region) of Figure A-2

$$C_h = r\left(\frac{\pi}{2}+1\right) \quad , \quad A_h = r^2\left(\frac{\pi}{2} - \theta - \sin\theta\cos\theta\right) \text{, and} \quad A_m = P\frac{t}{2} - A_h \tag{A-38}$$

where θ is given by Eq. (A-37). From Eq. (A-37) and (A-38) one obtains $\theta = 0.285$ rads, $C_h = 2.57r$, and $A_h = 1.016r^2$. For the cold channel

$$C_c = C_h \qquad \text{and} \qquad A_c = \frac{\pi}{2}r^2 - A_h \tag{A-39}$$

A.3 Boiler

The response of the two-phase mixture temperature in a counterflow heat exchanger to changes in boundary conditions is derived. It is assumed the hot side is single phase liquid and that the cold side has saturated liquid water entering and saturated steam exiting. If we assume the water is on the shell side, then the energy equation for the water is

$$\frac{d}{dt}M_{H_2O}\ i\ +\ \left(\rho V C_p\right)_{shell}\frac{d}{dt}T_{sat} = Q + w_{fw}h_{fw} - w_s h_g\ . \tag{A-40}$$

The above equation lumps the heat capacity of the shell in with the water mixture.

If we assume no change in mass so that the feedwater flow equals steam flow, then

$$\frac{d}{dt}M_{H_2O} = 0 = w_{fw} w_s\,, \tag{A-41}$$

and Eq. (A-40) becomes

$$\frac{di}{dt} + \frac{\left(\rho V\, C_p\right)_{shell}}{M_{H_2O}}\frac{d}{dt}T_{sat} = \frac{1}{M_{H_2O}}\left[Q - w_{fw}\left(h_g - h_{fw}\right)\right]. \tag{A-42}$$

The first term in Eq. (A-42) can be expanded into

$$\frac{d}{dt} i = c \frac{dT_{sat}}{dt} + i_{fg} \frac{d}{dt} x \tag{A-43}$$

where

$$c = (1 - x) \frac{d}{dT} i_f + x \frac{d}{dt} i_g \ . \tag{A-44}$$

Then Eq. (A-42) becomes

$$\left[c + \frac{\left(\rho V C_\rho \right)_{shell}}{M_{H_2O}} \right] \frac{d}{dt} T_{sat} + i_{fg} \frac{d}{dt} x = \frac{1}{M_{H_2O}} \left[Q - w_{fw} \left(h_g - h_{fw} \right) \right] . \tag{A-45}$$

The derivative of the quality with respect to time in this equation is eliminated next.

Writing the conservation of volume equation for the mixture

$$M_{H_2O} \frac{d}{dt} v = 0 \ , \tag{A-46}$$

where we have made use of Eq. (A-41). Expanding Eq. (A-46) leads to

$$0 = \phi \frac{d}{dt} T_{sat} + v_{fg} \frac{d}{dt} x \ , \tag{A-47}$$

where

$$\phi = x \frac{d}{dT} v_g + (1 - x) \frac{d}{dT} v_f \ . \tag{A-48}$$

The equation for the saturation temperature is obtained by combining Eqs. (A-45) and (A-47) which gives

$$\frac{d}{dt} T_{sat} = \frac{1}{M \left[c + \frac{\left(\rho V C_p \right)_{shell}}{M} - \frac{\phi i_{fg}}{v_{fg}} \right]} \left[Q - w_{fw} \left(h_g - h_{fw} \right) \right] . \tag{A-49}$$

If the change in T_{SAT} is small, then one can solve Eq. (A-49) with the properties and quality taken to be constant.

An expression for the heat transfer rate, Q, is obtained by assuming that the coolant axial temperature profiles are those that would result in the steady state given the instantaneous values of the boundary conditions. Then the log mean temperature model gives

$$\frac{T_{hi}-T_{sat}}{T_{ho}-T_{sat}} = exp\left[\frac{UA}{\left(wC_p\right)_h}\right] = K^{-1} \; . \tag{A-50}$$

and

$$Q = UA\,\frac{\left(T_{ho}-T_{sat}\right)-\left(T_{hi}-T_{sat}\right)}{\ln\left((T_{ho}-T_{sat})/(T_{hi}-T_{sat})\right)} \tag{A-51}$$

where the subscript h refers to the hot side, i to the inlet, and o to the outlet. Using the above equation and neglecting the thermal inertia of the hot side coolant, a hot side energy balance gives

$$Q = \left(w\ C_p\right)_h \left(1-K\right)\left(T_{hi}-T_{sat}\right) . \tag{A-52}$$

The final equation for the saturation temperature in terms of the time dependent boundary conditions of hot side inlet temperature, feedwater enthalpy, and steam flowrate is obtained by substituting Eq. (A-51) into Eq. (A-49) which gives,

$$\frac{d}{dt}T_{sat} = \frac{-1}{\tau}\left[T_{sat} + F\left(t\right)\right] \; , \tag{A-53}$$

where

$$\frac{1}{\tau} = \frac{\left(wC_p\right)_h\left(1-K\right)}{M_{H_2O}\left[c + \dfrac{\left(\rho V C_\rho\right)_{shell}}{M_{H_2O}} - \dfrac{\phi\, i_{fg}}{v_{vg}}\right]} \; . \tag{A-54}$$

A.4 Electrolytic Cell

The electrolytic cell modeled has a planar rectangular geometry consisting of the following components. Listed from cell exterior and moving through the cell in a line normal to the cell plane to the opposite side we have: steel separator, edge rails, porous cathode, electrolyte, porous anode, edge rails, and separator. The two inlet streams enter at right angles to each other with each stream entering along the normal to a cell edge. Of these components only the electrodes and electrolyte are in close contact with the gas streams and are sites of significant energy deposition/generation.

In modeling the cell note that the electrochemical processes reach equilibrium at a much faster rate than the thermal processes. It is reasonable then to model them as quasi-static. It is assumed that the two flow streams entering the cell do so at the same temperature. It is also assumed that the two flow streams within the interior of the cell are perfectly mixed and that each stream exits the cell at the same temperature. Further, the cell components listed above are all assumed to be in thermal equilibrium with each other and with the flow streams within the cell. Then an energy balance on the cell gives for the rate of change of cell temperature

$$\left[\left(\rho V C_p\right)_s + \left(\rho V C_v\right)_g\right] \frac{d}{dt} T =$$
$$\left[\begin{array}{c} m_{H_2O-i-cath}\, h_{H_2O}\,(T_i,P) + m_{H_2-i-cath}\, h_{H_2}(T_i,P) + m_{N_2-i-cath}\, h_{N_2}(T_i,P) + \\ m_{O_2-i-anode}\, h_{O_2}(T_i,P) + m_{N_2-i-anode}\, h_{N_2}(T_i,P) \end{array}\right] -$$
$$\left[\begin{array}{c} m_{H_2O-o-cath}\, h_{H_2O}\,(T,P) + m_{H_2-o-cath}\, h_{H_2}(T,P) + m_{N_2-o-cath}\, h_{N_2}(T,P) + \\ m_{O_2-o-anode}\, h_{O_2}(T,P) + m_{N_2-o-anode}\, h_{N_2}(T,P) \end{array}\right] + \qquad \text{(A-55)}$$
$$Q + W$$

where

ρ	=	density,
V	=	volume,
T	=	temperature,
m	=	species mass flow rate (kg/s),
h	=	specific enthalpy (joules/kg),
Q	=	rate of heat transfer to the electrolyzer,
W	=	rate of electrical work supplied to the electrolyzer, and
P	=	pressure,

and where subscripts *i* and *o* represent inlet and outlet, respectively, and *s* and *g* represent structure and gas, respectively. The electrical work is

$$W = V_{cell} \cdot A \cdot i = V_{cell} \cdot A \cdot \left(\frac{V_{cell} - V_N}{ASR}\right) \qquad \text{(A-56)}$$

where

V_{cell}	=	voltage applied to cell,
i	=	current density,
A	=	electrolyte area, and
ASR	=	area specific resistance,

and where

$$V_N = \frac{-1}{2F}\left[\Delta G_f{}^0(T) + RT \ln\left[\left(\frac{f_{H_2}\, f_{O_2}{}^{\frac{1}{2}}}{f_{H_2O}}\right)\left(\frac{P}{P_{STD}}\right)^{\frac{1}{2}}\right]\right] \qquad \text{and} \qquad \text{(A-57)}$$

$$ASR = \left(ASR\right)_0 + C_1 \exp\left(\frac{C_2}{T}\right). \tag{A-58}$$

The expression for V_N is from [7] and *C1* and *C2* are constants. In the last two equations T is in degrees K.

The characteristic times for how cell output quantities (species concentration, structure temperatures, and temperatures of gas streams) respond to changes in cell inlet conditions (current and inlet temperature) are derived for several simplifying and reasonable assumptions. The species concentrations and the gas stream temperatures respond much more quickly to changes in cell inlet conditions than do the temperatures of structures. These elements can be treated quasi-statically compared to the structures. Further, of the structures only the electrodes and electrolytes are in intimate contact with the changing thermal conditions in the cell. Assume that only water enters the cell and that only hydrogen and oxygen exit the cell. The heat capacity of the gas inside the cell is negligible and it is assumed the cell is operated adiabatically. Then from Eq. (A-55)

$$\rho V C_p \frac{d}{dt} T = m_{H_2O}\ h_{H_2O} - \left(m_{H_2} h_{H_2} + m_{O_2} h_{O_2}\right) + W \tag{A-59}$$

$$m_{H_2} = \frac{A_{H_2}}{A_{H_2O}} m_{H_2O} \qquad m_{o_2} = \frac{A_{O_2}}{2A_{H_2O}} m_{H_2O} \tag{A-60}$$

$$\rho V C_p \frac{d}{dt} T = m_{H_2O}\left[h_{H_2O}\left(T_i\right) - \frac{1}{A_{H_2O}}\left(A_{H_2} h_{H_2}\left(T\right) + \frac{A_{0_2}}{2}\left(T\right)\right)\right] + W \tag{A-61}$$

where ρ is the density and V is the volume and T is temperature of the electrodes and electrolyte (i.e. thermally active structures), m is species mass flow rate (kg/s), h is specific enthalpy (joules/kg), W is rate of electrical work supplied to the electrolyzer, A is atomic number, and subscript i represents inlet.

Suppose control on i (i.e. m_{H2}) and accept V_{cell}

$$m_{H_2O} = \frac{A_{H_2O} A}{2F} \tag{A-62}$$

Writing the electrical work in terms of current, i, Nernst voltage, V_N, cell area, A, and area specific resistance, *ASR,*

$$
\begin{aligned}
W &= V_{cell}\ A\ i \\
&= \left(V_N + i \cdot ASR\right) A\ i \\
&= AV_N\ i + A \cdot ASR\ i^2 \\
&= AV_N\left(T\right) i + A \cdot ASR\ i^2
\end{aligned}
\tag{A-63}
$$

$$
\begin{aligned}
\rho V C_p \frac{d}{dt} T = \frac{A_{H_2O} A}{2F}\ i \left[h_{H_2O}\left(T_i\right) - \frac{1}{A_{H_2O}} \left(A_{H_2}\ h_{H_2}\left(T\right) + \frac{A_{O_2}}{2} h_{O_2}\left(T\right) \right) \right] \\
+\ AV_N\left(T\right) i + A \cdot ASR\ i^2
\end{aligned}
\tag{A-64}
$$

and then linearizing the equation

$$
\begin{aligned}
\rho V C_p \frac{d}{dt} \delta T = {} & \frac{A_{H_2O} A}{2F} \left[i_o\ C_{\rho_{H_2O}} \delta T_i + h_{H_2O}\left(T_{i_o}\right) \delta i \right] \\
& - \frac{A A_{H_2}}{2F} \left[i_o\ C_{\rho_{H_2}}\ \delta T + h_{H_2}\left(T_o\right) \delta i \right] \\
& - \frac{A A_{O_2}}{4F} \left[i_o\ C_{\rho_{O_2}}\ \delta T + h_{O_2}\left(T_o\right) \delta i \right] \\
& + A \left[i_o \frac{\partial V_N\left(T\right)}{\partial T} \delta T + V_N\left(T_o\right) \delta i \right] \\
& + A \left[ASR_o \left(i_o^2 + 2 i_o \delta i + \left(\delta i\right)^2 \right) + i_o^2 \frac{\partial}{\partial T} ASR\ \delta T \right]
\end{aligned}
\tag{A-65}
$$

where subscript *o* represents the linearization point. The above equation gives the change in cell temperature (electrodes, electrolyte, and outlet gas streams) in terms of changes in cell current and temperature of the inlet gas streams. Collecting terms gives

$$
\begin{aligned}
\rho V C_\rho \frac{d}{dt} \delta T = {} & \frac{-i_o A}{2F} \left[A_{H_2} C_{\rho_{H_2}} + A_{O_2} C_{\rho_{O_2}} - 2F \frac{\partial V_N\left(T\right)}{\partial T} - 2F\ i_o\ \frac{\partial ASR}{\partial T} \right] \delta T \\
& + \frac{A}{2F} \left[A_{H_2O}\ h_{H_2O}\left(T_{i_o}\right) - A_{H_2} h_{H_2}\left(T_o\right) - \frac{A_{O_2}}{2} h_{O_2}\left(T_o\right) + 2F\ V_N\left(T_o\right) + 4F \cdot ASR\ i_o \right] \delta i \\
& + \left[\frac{A_{H_2O} A}{2F}\ i_o\ C_{\rho_{H_2O}} \right] \delta T_i
\end{aligned}
\tag{A-66}
$$

and from the above according to Eq. (4) the cell time constant is

$$\tau^{-1} = \frac{i_o A}{2F\left(\rho V C_\rho\right)_s}\left[A_{H_2}\ C_{\rho_{H_2}} + A_{O_2}\ C_{\rho_{O_2}} - 2F\ \partial\frac{V_{N(T)}}{\partial T} - 2F\ i_o\ \frac{\partial}{\partial T} ASR \right] \tag{A-67}$$

where the various terms in this equation are given by

$$V_N = +\frac{1}{2F}\left[\triangle G_f^o\left(T\right) + RT\ \ln\left\{ \left(\frac{f_{H_2} f_{o_2}{}^{1/2}}{f_{H_2O}} \right)\left(\frac{P}{P_{STD}} \right)^{1/2} \right\} \right] \tag{A-68}$$

$$\partial\frac{V_N}{\partial T} = +\frac{1}{2F}\left[\frac{\partial \triangle G_f^o}{\partial T} + R\ \ln\left\{ \left(\frac{f_{H_2} f_{o_2}{}^{1/2}}{f_{H_2O}} \right)\left(\frac{P}{P_{STD}} \right)^{1/2} \right\} \right] \tag{A-69}$$

$$ASR = ASR_o + C_1\ exp\left(\frac{C_2}{T} \right) \tag{A-70}$$

$$\partial\frac{ASR}{\partial T} = -\frac{C_1 C_2}{T^2}\ exp\left(\frac{C_2}{T} \right) = -\frac{C_2}{T}\left(ASR\right). \tag{A-71}$$

A.5 Pipe

The lumped-parameter temperature response of a volume of coolant in contact with structural material, such as a pipe or plenum wall, to a change in inlet temperature T_i or flowrate w of the coolant entering the volume, or to a change in structure temperature T_s is

$$\left(\rho V C_p\right)_{cl}\frac{d}{dt}T_{cl} = \left(wC_p\right)_{cl}\left(T_i - T_{cl}\right) + hA\left(T_s - T_{cl}\right) \tag{A-72}$$

or

$$\frac{d}{dt}T_{cl} = \frac{-1}{\tau_{cl}}\left[T_{cl} - F\left(t\right)\right], \qquad \tau_{cl} = \frac{\left(\rho V C_p\right)_{cl}}{\left(wC_p\right)_{cl} + hA}\ . \tag{A-73}$$

If the structure time constant is much faster than the coolant time constant, then the combined system has time constant

$$\tau = \frac{\left(\rho V C_p\right)_{cl} + \left(\rho V C_p\right)_s}{\left(wC_p\right)_{cl}}\ . \tag{A-74}$$

The pipe wall temperature, T_s, assuming a one-dimensional lumped node is given by

$$\left(\rho VC_p\right)_s \frac{d}{dt}T_s = -\left(hA\right)_{cl}\left[T_s - T_{cl}\right] \tag{A-75}$$

or

$$\frac{d}{dt}T_s = \frac{-1}{\tau_s}\left[T_s - T_{cl}\right], \qquad \tau_s = \left(\frac{\rho \Delta t C_p}{h}\right)_s \tag{A-76}$$

where

$$\frac{1}{h} = \frac{\Delta t}{2k} + \frac{1}{h_{cl}}\,. \tag{A-77}$$

In the above expression the first term is material conduction resistance and the second term is the film resistance.

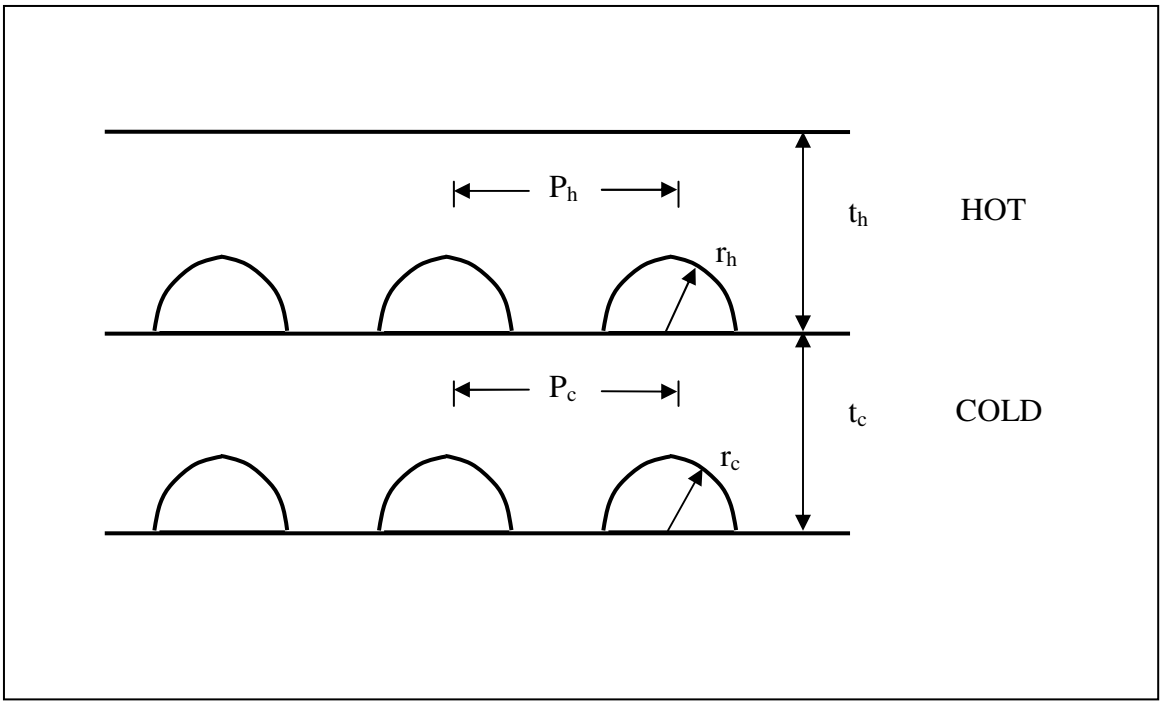

Figure A-1 View of Printed Circuit Heat Exchanger in Cross Section

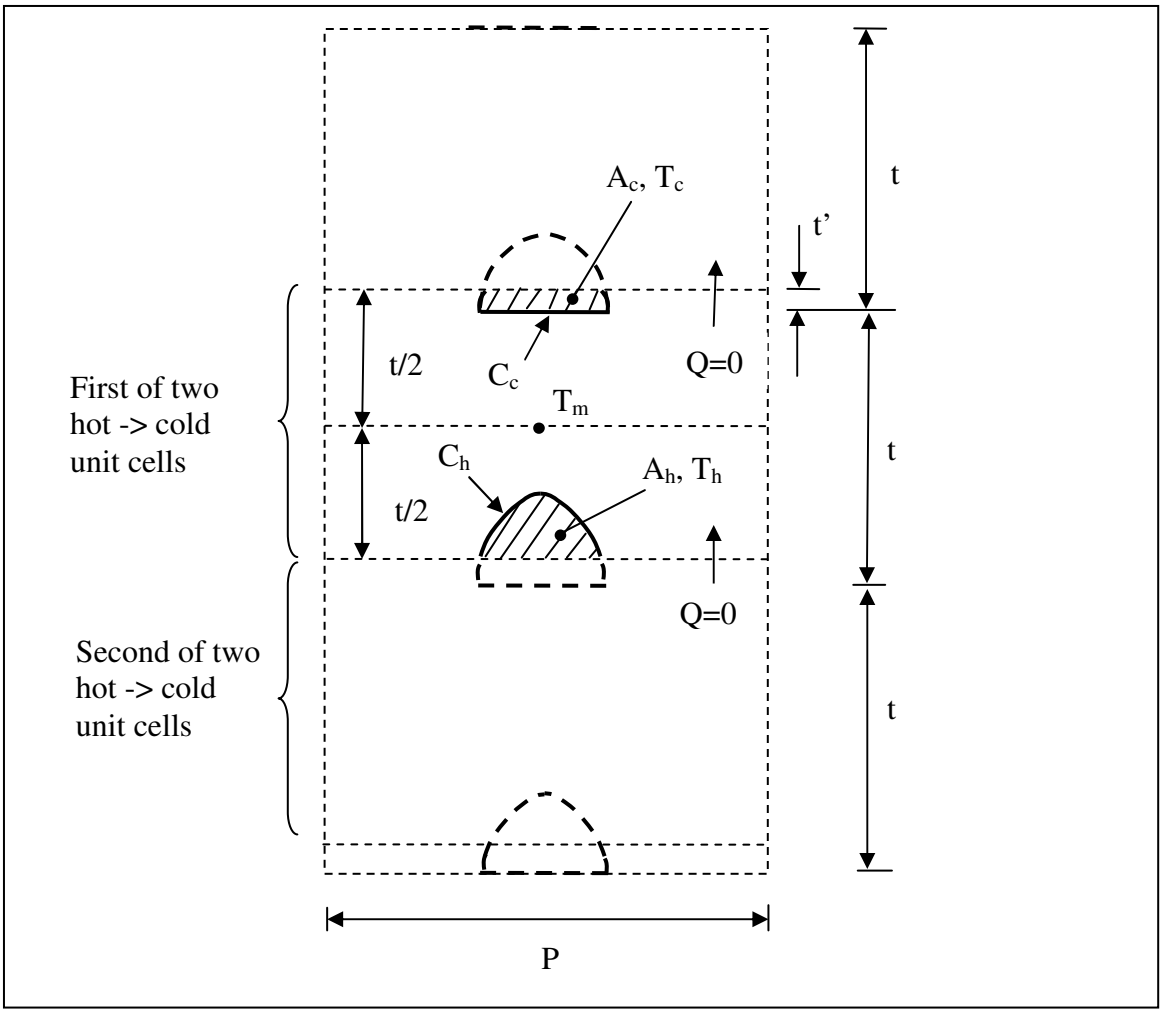

Figure A-2 Unit Cells Defined for Infinite Array of Hot and Cold Channels

APPENDIX B COMPONENT TIME CONSTANTS AND ENERGY CAPACITANCES

B.1. Reactor Neutronics and Heat Transfer

The development in Appendix A.1 and Table B-1 defines a unit cell consisting of fuel and moderator surrounding a single coolant channel. The unit cell is then represented by a solid cylinder cooled on the outside. This model gives a core heat transfer time constant of 9.6 s and an active core region energy capacitance of 200 MJ/C. These values appear in Table I.

It was shown in Appendix A.1 that the neutronic response to a change in reactivity is composed of a short and long-term response. When reactivity is added as a step, such as from a control rod, there is an adjustment to core power that takes place near instantaneously, i.e. the prompt jump. Then, as natural reactivity feedbacks act to null out the added reactivity, the core power changes with time constant given by Eq. (A-18). Given a one group precursor half life of $\lambda = 0.1\ s^{-1}$ and $A+B = -2.7\ \$$ from Table IV, the long term time constant for core power is 3.7 s. This value appears in Table II.

Note that the neutronic and heat transfer processes will tend toward a new equilibrium state one followed by the other, the order depending on whether the initial perturbation was to coolant temperature or to reactivity.

B.2 PCHE Heat Exchangers

As described previously there are incentives to choose printed circuit type heat exchangers for heat transfer circuits that use a gas coolant. In the reference configuration for the combined plant shown in Figure 3 the recuperator in the PCU and heat exchangers IHX and HTLHX are assumed to be PCHEs. Time constants and energy capacitances are calculated for these units from the models developed in Appendix A.2.

Design data for these heat exchangers are taken from [8] and are reproduced in Table B-3. Thermo-physical properties used in the calculation are given in Table B-4. Values for heat transfer parameters associated with the models of Appendix A.2 are given in Table B-5. The three time constants associated with the hot side of the PCHE are shown in Table B-6. Note that there are corresponding time constants not shown for the cold side. They were not calculated as their values will be similar to those for the hot side.

Inspection of Table B-6 shows that the heat exchanger metal has an energy capacitance at least five times greater than the next highest source of capacitance. The time constants associated with the other capacitances are at least a factor of ten faster than for the metal. Thus, the heat exchanger response is dominated by the metal behavior. Table B-7 shows the calculation of the metal capacitance. The cold side metal is accounted for by doubling the capacitance of the hot side metal. The time constants shown are those for the metal taken from Table B-6. This data is reproduced in Table II.

B.3. HTE Plant Heat Exchangers

The expression for the boiler time constant given by Eq. (A-54) is dependent on the internal geometry and dimensions of the heat exchanger. At this time the boiler design is known only to the level of thermal power and UA.[7] Rather than perform a detailed design effort to obtain this additional data, engineering scaling principles are applied to a unit for which a complete design is available. The unit is the 300 MWt Oconee once-through steam generator for which a dynamic model was developed in [9]. The temperatures and pressure conditions used in this model are similar to those in the HTE plant while the heat transfer rate is based on heat transfer correlations. So it is expected the numbers obtained should be representative for the purposes of scoping calculations.

The Oconee unit and related model [9] additionally have subcooled and superheat regions. It is advantageous then not limit to limit treatment of the time constant to just the boiler, but to set up a similar correspondence between HTE superheater and condenser components with once-through steam generator superheated and subcooled regions, respectively. Note that since the condensation heat rate in the HTE condenser in [7] is a small fraction of the component heat load, it will be ignored. The condenser can then be treated as a heat exchanger with subcooled water on one side and vapor on the other and data obtained from the subcooled region of the once-through steam generator.

In obtaining the heat exchanger data from the correspondences defined above, the assumption is made that the heat transfer coefficient in each of the superheater (HX1), boiler, and condenser in Figure 5 has the same value as in the corresponding regions of the Oconee model. This is a reasonable assumption since the underlying heat transfer mechanisms are the same between corresponding regions. In this case, individually for each region

$$\left(\frac{Q}{A\,\Delta T}\right)_{OT} = \left(\frac{Q}{A\,\Delta T}\right)_{HTSE} \tag{B-1}$$

where Q is the thermal power, A is the heat transfer coefficient, and ΔT is the log mean temperature difference and subscript OT represents once-through. The heat transfer areas are then related through

$$\frac{A_{HTSE}}{A_{OT}} = \left(\frac{Q}{\Delta T}\right)_{HTSE} \left(\frac{\Delta T}{Q}\right)_{OT}. \tag{B-2}$$

This scaling law is used to obtain HTE design data from the once-through design.

The area scaling factor on the left-hand side of the above equation is calculated for each of the HTE condenser, boiler, and superheater. These components appear in Figure 5 and the data used are from the HTE plant in [7] and the once-through unit in [9]. Note that the HTE plant contains superheaters HX1 and HX2 having thermal power 26 and 5 MWt,

respectively. For the purposes of computing time constants and energy capacitances, HX2 is ignored because its effect on time behavior is second order. The input data and the calculated values of the area scaling factor are shown in Table B-8. Note the expression for the log mean temperature difference, ΔT, differs between the single phase and two-phase cases.

In applying the area scaling factor to compute heat exchanger dimensions, it is assumed the adjusted area in going from once-through to HTE plant is achieved by changing only the number of heat exchanger tubes. Then the parameters shown in Table B-9 are assumed to remain constant. The number of tubes and the areas on either side of a HTE heat exchanger are shown in Table B-10 as derived by applying the scaling factor to the values of these same parameters in the once-through design. The energy capacitances are assumed to scale similarly. Values are given in Table B-11.

The values of the time constants for each of the superheater, boiler, and condenser in the HTE plant are given in Table B-12. These values are from the once-through steam generator in [9]. It has been assumed that in adjusting the areas from once-through to HTE the mass of coolant and structure and the flowrates change by the same factor. This will be true when the flowrates scale proportionally with power which would be the case if the log mean temperature difference remains unchanged. Since this is not exactly the case the time constant values from the once-through unit provide only approximate values.

The representative time constant and energy capacitance finally used for each HTE component was obtained as follows. Identified in Table B-11 in bold is the energy capacitance with the largest value among the four energy capacitances for each component. Note that each value is at least twice as big as the next largest value. To the first order then the time constant of the associated capacitance dominates. These time constants are taken as representative of the components and are shown in Table B-12 in bold. The bolded values are shown reproduced in summary in Table II.

B.4. Electrolytic Cell

The cell time constant (expression given in Appendix A) is evaluated for representative VHTR/HTSE cell conditions. For simplicity it was assumed the reactant stream is pure water vapor and that it is completely decomposed in the cell. The data input to the calculation are shown in Tables B-13 through B-15. It is assumed the reactant stream is pure water vapor and that it is completely decomposed by the cell as shown in Table B-13. Representative operating conditions are given in Table B-14. The values for cell mass and specific heat include only the electrodes and the electrolyte and not the separators, edge rails, or flow forms according to the rationale given earlier. The cell mass is from [10]. The ASR data is from [11]. The expression for the cell time constant (Eq. (A-54)) yielded for this data a value of 206 s.

The energy capacitance of the cell (expression given in Appendix A) is also evaluated for representative VHTR/HTSE cell conditions. The mass of a cell of electrode area 64 cm^2

as obtained from [10] was multiplied by the estimated specific heat of the cell material and the number of such cells to obtain the energy capacitance. The number of cells was obtained by taking the total electrode area from [7] and dividing by 64 cm^2. The calculation is shown in Table B-16 and yields a value of 270 J/K. It should be noted, however, that design optimization has not yet been performed and so electrode area is subject to some uncertainty. More aggressive operation of the cell could reduce total electrode area by up to a factor of ten compared to the value given in [7]. The estimated thermal capacitance would decrease by this same factor. The time constant and energy capacitance values have been entered in Table II.

The validity of assumptions made in the derivation of the one-dimensional model of Appendix A has been examined. The model ignores the two-dimensional nature of the temperature distributions in the electrodes, electrolyte, and gas streams that arise as a consequence of the planar rectangular geometry of the cell and the 90 degree difference in angle of incidence between the two gas streams. In addition the heat capacity of the steel separators and edge rails is neglected since their temperature state is thought to be not tightly thermally coupled to the electrodes and electrolyte.

An experiment [11] provided an opportunity to validate the expression for the time constant given by Eq. (A-67). In the experiment the identical Cerametec cell that is being used for water splitting SOEC studies at Idaho National Laboratory (INL) was run in fuel cell mode. The conditions are the same as in Table B-13 through B-15 with the exception that the pressure was atmospheric and that hydrogen and oxygen were fed into the cell rather than removed from the cell. The cell was operated at atmospheric pressure and hydrogen and oxygen were fed into rather than removed from the cell. The mole fractions of hydrogen, oxygen, and water estimated from [11] were 0.46, 0.2, and 0.85. The water-splitting model in Appendix A was modified to describe a fuel cell by a change of sign on the Nernst potential and the Gibbs standard free energy of formation (to account for interchange of products and reactants). With these adjustments and for the conditions in [11] Eq. (A-67) yields a cell time constant of 279 s.

A value for the time constant of the cell was derived from data in [11]. In the experiment the fuel cell was at a steady state prior to a step change in the cell current. The measured cell outlet temperature during the subsequent transient appears in Figure B-1. The description in [11] indicates there was an initial power supply problem and, hence, the appearance of a saw tooth on the ramp up in temperature. We have attempted to adjust for this by backward extrapolating in time after the occurrence of the sawtooth. Figure B-1 shows the back calculation of a value for the time constant from the experiment data. The value from Eq. (A-67) (i.e. 279 s as given above) differs by 19 percent from the value of 235 s obtained from Figure B-1. This suggests that the assumptions underlying the derivation in Appendix A are reasonable from the standpoint of estimating an approximate measure of cell outlet temperature time response.

B.5 Pipes to/from HTE Process

Dimensions for the pipes to and from the HTE process are for FLINAK and a distance of 90 m.[14] Time constants are from Eqs. (A-74) and (A-76). Data is given in Table B-17.

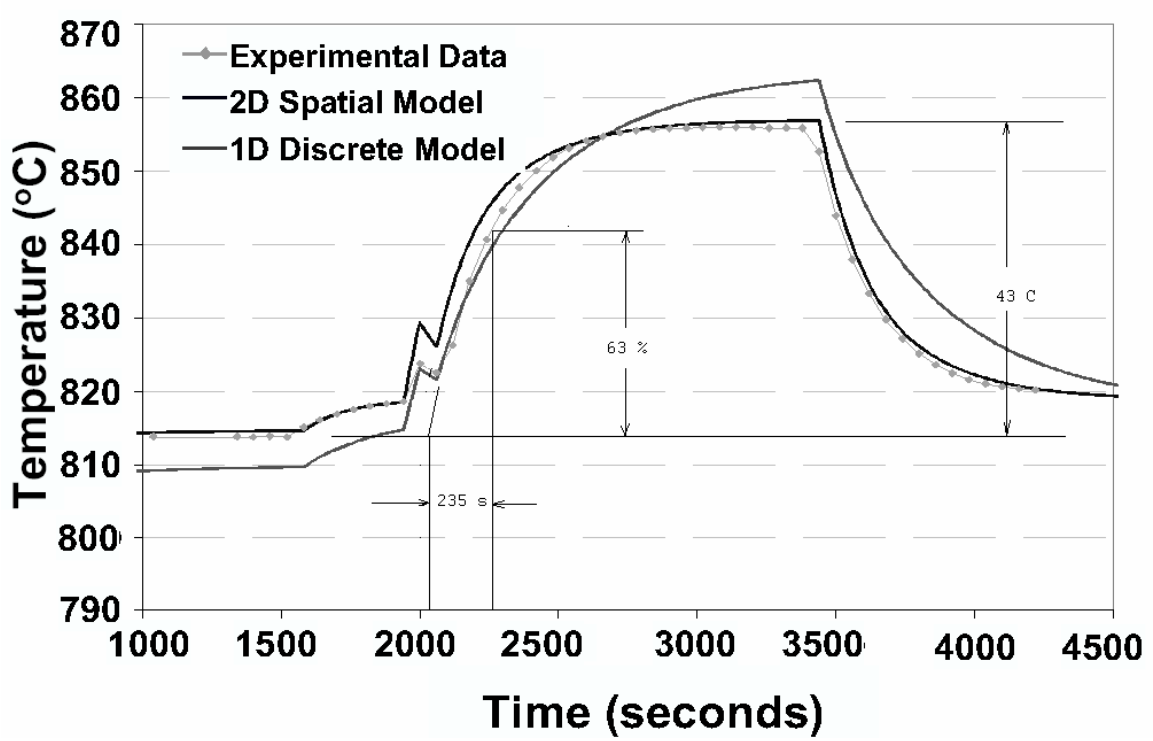

Figure B-1 Time Constant for an Electrolytic Cell Operating in the Fuel Cell Mode

Table B-1 Thermal Time Constant and Capacitance of Fuel Element as Represented by Solid Cylinder

Volume per Fuel Element	Exterior Volume (m^3)	Coolant Volume (m^3)	Fuel Matrix Volume, (m^3)	Graphite Volume, (m^3)
	$\sqrt{3}(0.360)^2\ 0.79 = 0.177$	$108 \cdot 0.79 \cdot \frac{\pi}{4} \cdot 0.016^2 = 0.017$	$210 \cdot 0.79 \cdot \frac{\pi}{4} \cdot 0.0127^2 = 0.021$	0.177-0.017-0.021 = 0.139
Volume per Coolant Hole	Coolant Volume, V_{cl} (m^3)	Fuel Matrix Volume, V_f (m^3)	Graphite Volume, V_c (m^3)	
	0.017/108 = 0.157e-3	0.021/108 = 0.194e-3	0.139/108 = 1.29e-3	
Mass per Fuel Element	UO_2 Mass (Kg)	UC_2 Mass (Kg)	C Mass (Kg)	
	~2350/720 = 3.26	~2350/720 = 3.26	0.139·1740 = 242	
Mass per Coolant Hole	m_{UO_2} (Kg)	m_{UC_2} (Kg)	m_C (Kg)	
	3.26/108 = 0.030	3.26/108 = 0.030	242/108 = 2.24	
Density	$\rho_{UO_2}\ (Kg/m^3)$	$\rho_{UC_2} \sim \rho_{UC}\ (Kg/m^3)$	$\rho_C\ (Kg/m^3)$	
	11,000	13,600	1,740	
Specific Heat	Cp_{UO_2} (J/Kg-c)	$Cp_{UC_2} \sim Cp_{UC}$ (J/Kg-C)	Cp_C (J/Kg-C)	
	300	160	1100	
Conductivity	k_C (W/m-K)	k_{He} (W/m-K)		
	80	0.37		
Thermal Capacitance per Coolant Hole	$(mC_\rho)_{UO_2} + (mC_\rho)_{UC_2} + (mC_\rho)_C$ (J/°C)			
	0.03·300+0.03·160+2.24·1100 = 2500			
Equivalent Radius of Solid per Coolant Hole	L (m)	$V = V_C + V_f$ (m^3)	$r = \left(\frac{V}{\pi L}\right)^{1/2}$ (m)	
	0.79	(1.29+0.194)e-3 = 1.48e-3	0.024	

Table B-1 Thermal Time Constant and Capacitance of Fuel Element as Represented by Solid Cylinder (cont'd)

Coolant Heat Transfer Coefficient	$(Re)_{He}$	$(Pr)_{He}$	D_{cl} (m)	$h_{cl} = \frac{k_{He}}{D_{cl}} 0.023\ \mathrm{Re}^{0.8}\ \mathrm{Pr}^{0.3}$ (W/m^2-C)
	41,000	-1	0.016	2600
Effective Heat Transfer Coefficient (J/s-m-C)	$h = \left(\frac{r}{4k_C} + \frac{1}{h_{cl}} \right)^{-1}$			
	$\left(\frac{0.024}{4.80} + \frac{1}{2600} \right)^{-1} = 2200$			
Fuel Element Time Constant (s)	$\tau = \frac{\rho V C_p}{2\pi rhL}$, (s) Eq.(x)			
	$\frac{2500}{2\pi \cdot 0.024 \cdot 2200 \cdot 0.79} = 9.5$			
Active Core Energy Capacitance (J/C)	$\left[\left(mC_\rho\right)_{UO_2} + \left(mC_\rho\right)_{UC_2} + \left(mC_\rho\right)_C \right] \cdot N_{holes} \cdot N_{elements}$			
	$2500 \cdot 108 \cdot 720 = 200e6$			

Table B-2 Upper Bound for Differential Worth of Operating Control Rods for GT-MHR

Number of Operating Control Rods[a] i.e., outer neutron control	36
Upper limit on worth per rod[b] ($)	0.5
Absorber length of Operating Control Rod[c] (in/m)	229/5.8
Worth per absorber per unit absorber length ($/m)	0.5/5.8=0.086
Combined worth of Operating Control Rods per unit absorber length ($/m)	0.086(36) = 3.1

[a] Startup control rods are withdrawn before criticality: p.4-5 and p. 4-12 of [13].
Operating control rods are inserted to varying heights during operation: p.4-22 of [13].
[b] Each control rod has its own independent drive: p.4-26 of [13]. Any single drive, for safety reasons, should be limited to less then one dollar.
[c] Figs. 4.1-12, 4.1-13, and 4.2-2 [13]. Scaled from these figures.

Table B-3 Design Data for Helium Printed Circuit Heat Exchangers [8]

	IHX	HTLHX	PCU Recuperator
Channel Diameter, $2r$ (m)	1.5e-03	1.5e-03	1.5e-03
Channel Pitch, P (m)	1.8e-03	2.25e-03	2.56e-03
Plate Thickness, t (m)	8.55e-04	1.17e-03	1.79e-03
Channel Length, l (m)	2.34	1.089	1.62
Number of Channels, $N_{channels}$ (one side)	7.33e06	4.36e05	4.264e06
In Width Direction	2639	673	2443
In Height Direction	2778	648	1745
Hot Side Flow, w (kg/s) - Total	289	32.1	260
$w_{channel}$ - Per Channel	3.94e-05	7.36e-05	6.10e-05
Cold Side Flow, w (kg/s) - Total	292	27.5	260
$w_{channel}$ - Per Channel	3.98e-05	6.31e-05	6.10e-05
Width (m)	4.75	1.52	6.23
Height (m)	4.75	1.52	6.23
Volume (m^3)	52.8	2.5	62.9

Table B-4 Thermo-Physical Properties for Helium Printed Circuit Heat Exchangers

	IHX	HTLHX	PCU Recuperator
$(C_p)_m$ (J/kg-K)	500	500	500
$(C_v)_h = (C_p)_h - R$ (J/kg-K)	3114	3114	3114
$(C_p)_h$ (J/kg-K)	5200	5200	5200
ρ_h (kg/m^3)	3.59	3.47	2.18
ρ_m (kg/m^3)	8000	8000	8000
k_m (J/m-s-K)	22	23	16.4

Table B-5 Hot-Side Heat Transfer Parameters for Helium Printed Circuit Heat Exchangers

	IHX	HTLHX	PCU Recuperator
θ (rads), Eq. (13)	0.285	0.285	0.285
C_h (m), Eq. (14)	0.00193	0.00193	0.00193
A_h (m^2), Eq. (14)	5.71e-07	5.71e-07	5.71e-07
h_{h-m} (J/m-s-K) (Ref. C. Oh)	1660	1715	2089
$\bar{h}_{h-m}$ (J/m-s-K), Eq. (4)	2.82	3.1	3.61
A_m (m^2)	1.98e-07	7.45e-07	1.72e-06

Table B-6 Time Constants for Helium Printed Circuit Heat Exchangers

	IHX	HTLHX	PCU Recuperator
$(\rho A l C_v)_h$ (joules/°C)	0.0150	0.00672	0.00628
$(C_p w)_h$	2.05e-01	3.83e-01	3.17e-01
$(\rho A C_v)_h$	0.00638	0.00617	0.00388
$(\rho A C_p)_m$	7.94e-01	2.98	6.88
$\tau_{i-h} = \frac{(\rho A l C_v)_h}{(C_p w)_h}$ (s)	0.07	0.02	0.02
$\tau_{h-m} = \frac{(\rho A C_v)_h}{\bar{h}_{h-m}}$ (s)	0.002	0.002	0.001
$\tau_{m-h} = \frac{(\rho A C_p)_m}{\bar{h}_{h-m}}$ (s)	0.28	0.96	1.9

Table B-7 PCHE Time Constant and Energy Capacitance

	IHX	HTLHX	PCU Recuperator
Metal Energy Capacitance $(\rho A C_p)_m$ per channel (J/C-m)	7.94e-01	2.98	6.88
Channel Length, l (m)	2.34	1.089	1.62
Number of Channels, $N_{channels}$ (one side)	7.33e06	4.36e05	4.264e06
Total Capacitance, $2\ (\rho A C_p)_m\ l\ N_{channels}$ (MJ/C)	27	2.8	95
Dominant Time Constant	0.28	0.96	1.9

Table B-8 Area Factor for Scaling from 300 MWt Oconee Once-Through Steam Generator to HTE Water Heat Exchangers

Region-to-Component Correspondence		Q (MWt)		T_{hi} (C)		T_{ho} (C)		T_{ci} (C)		T_{co} (C)		ΔT (C)			$\frac{A_{HTE}}{A_{OT}}$
OT Region	HTE Component	OT [x]	HTE [x]	OT	HTE	OT	HTE	OT	HTE	OT	HTE	Eq.()	OT	HTE	
Subcooled	Condenser*	16	15.4	303	304	293	68	266	21	286	182	18a	21	79	0.26
Two-Phase	Boiler	244	43.4	452	500	303	339	286	257	286	257	19a	65	148	0.078
Superheated	HX1	40	26	476	989	452	540	286	257	347	742	18a	147	264	0.36

* Vapor condensing on hot side is small part of total heat load so hot side behaves very nearly as a single phase coolant

Table B-9 Dimensions Preserved in Scaling from Once-Through Steam Generator to HTE Water Heat Exchangers

Parameter	Value [9]
Tube Length (m)	
Subcooled/Condenser	1.14
Two-Phase/Boiler	0.86
Superheater/HX1	1.00
Tube Outside Diameter (m)	1.67E-02
Tube Inside Diameter (m)	1.27E-02
Tube Pitch-to-Diameter ratio	1.355
Shell Thickness	2.0E-02

Table B-10 HTE Water Heat Exchanger Dimensions Scaled from 300 MWt STAR-LM Once-Through Steam Generator

Water Phase Region-to-Component Correspondence		Number of Tubes		Flow Area on Water Side (m^2)		Flow Area on Non-Water Side (m^2)*	
STAR-LM Region	HTE Component	STAR-LM	HTE	STAR-LM	HTE	STAR-LM	HTE
Subcooled	Condenser	26720	6900	5.99	1.6	3.39	0.88
Two-Phase	Boiler	26720	2100	5.99	0.47	3.39	0.26
Superheated	HX1	26720	9600	5.99	2.2	3.39	1.2

* Based on coolant with specific heat and heat transfer properties of PbBi

Table B-11 HTE Water Heat Exchanger Energy Capacitances Scaled from 300 MWt STAR-LM Once-Through Steam Generator

Water Phase Region-to-Component Correspondence		Energy Capacitance of Shell Structure on Water Side (MJ/C)		Energy Capacitance of Tube Structure on Non-Water Side (MJ/C)		Energy Capacitance of Water in Contact with Shell (MJ/C)		Energy Capacitance of Coolant in Contact with Tube (MJ/C)*	
STAR-LM Region	HTE Component	STAR-LM	HTE	STAR-LM	HTE	STAR-LM	HE	STAR-LM	HTE
Subcooled	Condenser	7	1.8	14	3.6	27	**7.0**	6	1.6
Two-Phase	Boiler	5	0.40	11	0.86	29	**2.3**	4	0.31
Superheated	HX1	6	2.2	12.4	**4.5**	1.4	0.50	5	1.8

*Based on coolant with specific heat and heat transfer properties of PbBi

Table B-12 HTE Water Heat Exchanger Time Constants from 300 MWt STAR-LM Once-Through Steam Generator

	Shell Structure (s)	Tube Structure (s)	Water in Contact with Shell (s)	Coolant in Contact with Tube* (s)
Condenser	179	14	**30**	0.4
Boiler	42	1.8	**20**	0.4
HX1	417	**35**	1.3	0.4

*Based on coolant with specific heat and heat transfer properties of PbBi

Table B-13 Species Data for Electrolytic Cell Time Constant Estimate

	H_2O	H_2	O_2
A_w (kg/mol)	18.0e-3	2.02e-3	32.0e-3
C_ρ @ 950°C (J/kg-K)	2.45e+3 @50 atm	15.1e3 @1 atm	917 @1 atm
f	1.0	0.67	0.33

Table B-14 Operating Data for Electrolytic Cell Time Constant Estimate

A (m^2)	i (amps/m^2)	$(\rho V)_s$[c] (kg)	$(C_\rho)_s$ (J/kg-K)	P/P_{STD}	T (C)
64e-4	1880	13.9e-3	400	50	816

[a]J. Hartivigsen

Table B-15 Other Data for Electrolytic Cell Time Constant Estimate

F (coul/mol)	R (J/mol-K)	$\frac{(\partial \Delta G)^o}{\partial T}$ [a] (J/mol-K)	ASR_o [b] (ohms-cm^2)	C_1 [b] (ohms-m^2)	C_2 [b] (K)	ΔG^o [a] (J/mol)
96,485	8.31	-55.5 @1 atm, 950°C	0	8.39e-4	8,030	2.02e5 @1 atm, 950°C

[a][12] [b][11] [c][10] (electrodes and electrolyte)

Table B-16 Electrolytic Cell Time Constant and Energy Capacitance

τ (s)	Cell area = 225 cm^2		Cell area =64 cm^2		
	No. of cells[b]	Stack Electrode Area[b] (m^2)	No. of Cells	$(\rho V)_s (C_\rho)_s$ per Cell (J/K)	Total[a] $(\rho V)_s (C_\rho)_s$ (J/K)
206	14e06	0.0225*14e06= 3.15e5	3.15e5/0.0064= 49.2e06	13.9e-03*400= 5.56	5.56*49.2e06= 270e06

[a] Electrodes and electrolyte only [b] Values from GAS-PASS/H simulation in [7]

Table B-17 Time Constants and Energy Capacitances of Coolant and Wall of Pipes to/from HTE Plant. FLINAK and separate hot/cold legs.

Pipe Dimensions	Length, L (m)	Inner Radius, r_i (m)	Outer Radius, r_o (m)	Flowrate, w (kg/s)	Velocity, v (m/s)		
	90	0.065	0.079	133	5.3		
Coolant	μ (Pa-s)	C_p (J/C-kg)	k (W/m-C)	ρ (kg/m^3)	Re	Pr	$h_{cl} = \frac{k_{He}}{D_{cl}} 0.023\ \mathrm{Re}^{0.8}\ \mathrm{Pr}^{0.3}$ (W/m^2-C)
	1.62E-03	1905	0.8	1880	8.0E05	3.9	1.1E04
Structure	k (W/m-C)	C_p (J/C-kg)	ρ (kg/m^3)				
	25	500	8000				
$\frac{1}{h} = \frac{\Delta t}{2k} + \frac{1}{h_{cl}}$ (W/m^2-C)	2700						
Time Constants and Energy Capacitances	$\tau_s = \left(\frac{\rho \Delta t C_p}{h} \right)_s$ (s)	$\tau_{cl} = \frac{\left(\rho V C_p\right)_{cl}}{\left(w C_p\right)_{cl} + hA}$ (s)	$\left(\rho V C_p\right)_s$ (MJ/C)	$\left(\rho V C_p\right)_{cl}$ (MJ/C)			
	21	12	2.3	4.3			

Nuclear Engineering Division
Argonne National Laboratory
9700 South Cass Avenue, Bldg. 208
Argonne, IL 60439-4842
www.anl.gov

UChicago ▶ Argonne LLC

A U.S. Department of Energy laboratory
managed by UChicago Argonne, LLC